

INVESTIGATING THE PHOTOINITIATED POLYMERIZATION KINETICS OF
THIOXANTHONE ACETIC ACID DERIVATIVES: A COMPUTATIONAL STUDY

by

Eyüp Metin

B.S., Chemistry, Yıldız Technical University, 2016

Submitted to the Institute for Graduate Studies in
Science and Engineering in partial fulfillment of
the requirements for the degree of
Master of Science

Graduate Program in Chemistry

Boğaziçi University

2019

To my family...

ACKNOWLEDGEMENTS

First of all, I would like to present my special thanks to my supervisor Assoc. Prof. Şaron Çatak and co-supervisor Prof. Viktorya Aviyente for their guidance, support and help. Being their student has been an honor.

I wish to extend my thanks to my bachelor supervisor Prof. Nergis Arsu for her support, encouragement and also contributing to this study.

I thank all the current and former members of CCBG for their friendship.

Moreover, I express my deepest thanks to my best friends; Ayhan Demirok, Emir Öztürk, Mert Bağbaşı and Soner Varol for their invaluable friendship.

I specially thank one of my best friends and colleague Res. Asst. Burak Evren for his encouragement and making our job joyful in all circumstances.

I would also like to thank my cousin Orhan Metin for being a brother to me, for his continuous support and trust.

I would like to present my gratitude to my dearest Gönül S. Batıbay, for always standing by my side, sharing the happiness and sadness, for believing in me, motivating me and making me feel safe.

Lastly, I would like to present my gratitude and appreciation to my parents, Kazım Metin and Fatma Metin. They have only one dream; seeing me happy. I am grateful to them for making me happy with all means they could offer. No matter what the issue was; they have never stopped supporting and being there for me. This dissertation is the result of this everlasting support and love.

ABSTRACT

INVESTIGATING THE PHOTOINITIATED POLYMERIZATION KINETICS OF THIOXANTHONE ACETIC ACID DERIVATIVES: A COMPUTATIONAL STUDY

In this study, we have investigated the kinetic and thermodynamic parameters of the initiation reactions of two well-known photoinitiator types; *One-Component Type II* and conventional *Type II*. Density Functional Theory (DFT) has been used in all calculations. The most suitable methodology for thioxanthone acetic acid based photoinitiators has been chosen by assessing the level of theory. Absorption spectra of thioxanthone acetic acid derivatives have been generated by Time-Dependent Density Functional Theory (TD-DFT). Dynamic and vibrational effects have been included in the calculations by including the Wigner methodology. Calculated absorption spectra have been compared with the experimental absorption spectra of thioxanthone acetic acid derivatives. In order to understand the nature of electronic transitions, Natural Transition Orbitals (NTOs) have been generated and the ϕ_S index values have been calculated. Competition between the thioxanthone acetic acid based exocyclic and endocyclic radicals, which co-exist in the reaction media, have been evaluated. Furthermore, initiation efficiencies of phenyl acetic acid based radicals and thioxanthone acetic acid based radicals have been compared in terms of their kinetic and thermodynamic parameters. In order to assess the radical reactivity, spin densities and radical Fukui functions have been calculated.

ÖZET

TİYOKZANTON ASETİK ASİT TÜREVLERİNİN FOTOBAŞLATILMIŞ POLİMERİZASYON KİNETİK ÖZELLİKLERİNİN İNCELENMESİ: HESAPSAL BİR ÇALIŞMA

Bu çalışmada, iki farklı çok iyi bilinen fotobaşlatıcı tipi olan *Tek-Bileşenli Tip II* ve geleneksel *Tip II* fotobaşlatıcıların başlatma reaksiyonlarının kinetik ve termodinamik parametreleri incelenmiştir. Tüm hesaplamalarda Yoğunluk Fonksiyonel Teorisi (DFT) kullanılmıştır. Tiyokzanton asetik asit bazlı fotobaşlatıcılara en uygun yöntem teori düzeyinin değerlendirilmesi ile belirlenmiştir. Tiyokzanton asetik asit türevlerinin soğurma spektrumları Zamana-Bağlı Yoğunluk Fonksiyonel Teorisi (TD-DFT) kullanılarak oluşturulmuştur. Dinamik ve titreşimsel etkiler Wigner dağılım metodu ile hesaplamalara dahil edilmiştir. Hesaplanan soğurma spektrumları tiyokzanton asetik asit türevlerinin deneysel soğurma spektrumları ile karşılaştırılmıştır. Elektronik geçişlerin doğasını anlamak için Doğal Geçiş Orbitalleri (NTO) oluşturulmuş ve ϕ_S belirteci değerleri hesaplanmıştır. Reaksiyon ortamında aynı anda bulunan halka içi ve halka dışı tiyokzanton asetik asit bazlı radikallerin rekabeti incelenmiştir. Ayrıca fenil asetik asit bazlı radikaller ile tiyokzanton asetik asit bazlı radikallerin başlatma etkinlikleri kinetik ve termodinamik parametreleri ile kıyaslanmıştır. Radikal reaktivliğinin belirlenmesi amacıyla spin yoğunlukları ve radikal Fukui fonksiyonları hesaplanmıştır.

TABLE OF CONTENTS

ACKNOWLEDGEMENTS	iv
ABSTRACT	v
ÖZET	vi
LIST OF FIGURES	ix
LIST OF TABLES	xii
LIST OF SYMBOLS	xv
LIST OF ACRONYMS/ABBREVIATIONS	xvii
1. INTRODUCTION	1
1.1. Photochemistry	1
1.1.1. Jablonski Diagram and Electronic Transitions	2
1.2. Photoinitiators	5
1.2.1. <i>Type I</i> Photoinitiators	7
1.2.2. <i>Type II</i> Photoinitiators	8
1.2.3. <i>One-Component Type II</i> Photoinitiators	10
1.2.4. Thioxanthenes as Photoinitiators	12
2. METHODOLOGY	14
2.1. Density Functional Theory	16
2.2. Functionals	18
2.3. Basis Sets	21
2.4. Time-Dependent Density Functional Theory	22
2.5. Polarizable Continuum Model	24
2.6. Wigner Distribution Function	26
2.7. ϕ_S Index	28
2.8. Fukui Functions	30
3. AIM OF THE STUDY	32
4. RESULTS	33
4.1. Computational Procedure	33
4.2. Background	34
4.3. Assessing the Level of Theory	39

4.3.1. Energetics	39
4.3.2. Vertical Excitations	42
4.4. Absorption Properties and Frontier Orbitals	44
4.5. Natural Transition Orbitals	50
4.6. Kinetic and Thermodynamic Properties of Reactions	55
4.6.1. Radical Formation Reactions	55
4.6.2. Initiation Reactions	57
5. CONCLUSION	66
REFERENCES	68
APPENDIX A: GROUND STATE GEOMETRIES	79

LIST OF FIGURES

Figure 1.1.	Electromagnetic spectrum and its regions.	2
Figure 1.2.	Jablonski diagram.	3
Figure 1.3.	<i>Type I</i> radical formation reaction.	7
Figure 1.4.	Structure of α -hydroxyketone.	8
Figure 1.5.	<i>Type I</i> radical formation reaction of Irgacure 2959.	8
Figure 1.6.	Structures of benzophenone, xanthone and thioxanthone.	9
Figure 1.7.	<i>Type II</i> radical formation reaction of thioxanthone.	9
Figure 1.8.	Examples of co-initiators in <i>Type II</i> reactions.	10
Figure 1.9.	Synthesis of thioxanthone and its derivatives.	11
Figure 1.10.	<i>One-Component Type II</i> radical formation reaction of TX-SH. . .	11
Figure 1.11.	Molecule structures of thioxanthone and phenyl acetic acid derivatives.	13
Figure 2.1.	Illustration of implicit and explicit solvation models.	25
Figure 2.2.	Wigner function graph $W(x,p)$, illustrating the momentum and the position probability distribution.	28

Figure 2.3.	Graphical illustration of ϕ_S index as the overlap between detachment and attachment density matrices.	30
Figure 4.1.	Experimentally proposed radical formation reaction of TX-AA. . .	34
Figure 4.2.	Experimentally proposed radical formation reaction of TX-NH-AA, TX-O-AA and TX-S-AA.	35
Figure 4.3.	Radical formation reaction of PHC.	36
Figure 4.4.	Radical formation reaction of PHN, PHO and PHS.	36
Figure 4.5.	Initiation reactions modeled in this study (X:NH, O, S).	38
Figure 4.6.	Free energy of activation with different functionals in the exocyclic radical attack to MMA reactions of thioxanthone acetic acid derivatives.	40
Figure 4.7.	Ground state geometries of thioxanthone acetic acid derivatives (a) TX-AA, (b) TX-NH-AA, (c) TX-O-AA and (d) TX-S-AA.	44
Figure 4.8.	Calculated and experimental UV-Vis absorption spectra of TX-NH-AA.	47
Figure 4.9.	Calculated and experimental UV-Vis absorption spectra of TX-AA.	47
Figure 4.10.	Calculated and experimental UV-Vis absorption spectra of TX-O-AA.	48
Figure 4.11.	Calculated and experimental UV-Vis absorption spectra of TX-S-AA.	48

Figure 4.12. Overall radical formation reactions of (a) thioxanthone acetic acid derivatives and (b) phenyl acetic acid derivatives (X:NH, O, S).	56
Figure 4.13. PES of TX-AA _{exo} radical attack to MMA.	60
Figure 4.14. PES of TX-AA _{endo} radical attack to MMA.	60
Figure 4.15. Radicalic centers in initiation reactions of (a) and (b) thioxanthone acetic acid derivatives and (c) phenyl acetic acid derivatives.	61
Figure 4.16. Correlation between spin densities and ΔG^\ddagger of thioxanthone based initiating radicals.	63
Figure 4.17. Correlation between radical Fukui function and ΔG^\ddagger of thioxanthone based initiating radicals.	63
Figure 4.18. Correlation between spin densities and ΔG^\ddagger of thioxanthone and phenyl acetic acid based initiating radicals.	64
Figure 4.19. Correlation between radical Fukui function and ΔG^\ddagger of thioxanthone and phenyl acetic acid based initiating radicals.	64

LIST OF TABLES

Table 1.1.	Electronic transition types, their selection rules and corresponding absorption strengths of carbonyl group.	4
Table 4.1.	Relative Gibbs energies (kcal/mol) for the transition states, intermediates and PRCs in the reactions of exocyclic radical attack to MMA.	41
Table 4.2.	Singlet Excitation Properties of TX-AA with different methodologies.	43
Table 4.3.	Singlet Excitation Properties of TX-NH-AA with different methodologies.	43
Table 4.4.	Singlet Excitation Properties of TX-O-AA with different methodologies.	43
Table 4.5.	Singlet Excitation Properties of TX-S-AA with different methodologies.	44
Table 4.6.	Singlet excitation properties of thioxanthone acetic acid derivatives (B3LYP/6-31+G(d,p) for S: 6-311++G(3df,3pd) in DMF).	45
Table 4.7.	Frontier orbitals of thioxanthone acetic acid derivatives (B3LYP/6-31+G(d,p) for S: 6-311++G(3df,3pd) in DMF).	49
Table 4.8.	Occupied and virtual NTOs of TX-AA with calculated parameters of transitions (B3LYP/6-31+G(d,p) for S: 6-311++G(3df,3pd) in DMF).	51

Table 4.9.	Occupied and virtual NTOs of TX-NH-AA with calculated parameters of transitions (B3LYP/6-31+G(d,p) for S: 6-311++G(3df,3pd) in DMF).	52
Table 4.10.	Occupied and virtual NTOs of TX-O-AA with calculated parameters of transitions (B3LYP/6-31+G(d,p) for S: 6-311++G(3df,3pd) in DMF).	53
Table 4.11.	Occupied and virtual NTOs of TX-S-AA with calculated parameters of transitions (B3LYP/6-31+G(d,p) for S: 6-311++G(3df,3pd) in DMF).	54
Table 4.12.	Overall reaction Gibbs free energies (ΔG_{rxn}^o , kcal/mol) of radical formation.	56
Table 4.13.	Kinetic and thermodynamic parameters of exocyclic and endocyclic radical attack reactions of thioxanthone and phenyl acetic acid derivatives.	58
Table 4.14.	Spin densities and radical Fukui function values of initiating radicals and spin densities of the intermediates calculated with NPA (B3LYP/6-31+G(d,p) for S: 6-311++G(3df,3pd) in DMF).	62
Table A.1.	Optimized ground state geometries of TX-AA _{exo} radical attack to MMA (B3LYP/6-31+G(d,p) for S: 6-311++G(3df,3pd) in DMF).	80
Table A.2.	Optimized ground state geometries of TX-NH-AA _{exo} radical attack to MMA (B3LYP/6-31+G(d,p) for S: 6-311++G(3df,3pd) in DMF).	81
Table A.3.	Optimized ground state geometries of TX-O-AA _{exo} radical attack to MMA (B3LYP/6-31+G(d,p) for S: 6-311++G(3df,3pd) in DMF).	82

Table A.4.	Optimized ground state geometries of TX-S-AA _{exo} radical attack to MMA (B3LYP/6-31+G(d,p) for S: 6-311++G(3df,3pd) in DMF). .	83
Table A.5.	Optimized ground state geometries of TX-AA _{endo} radical attack to MMA (B3LYP/6-31+G(d,p) for S: 6-311++G(3df,3pd) in DMF). .	84
Table A.6.	Optimized ground state geometries of TX-NH-AA _{endo} radical attack to MMA (B3LYP/6-31+G(d,p) for S: 6-311++G(3df,3pd) in DMF). .	85
Table A.7.	Optimized ground state geometries of TX-O-AA _{endo} radical attack to MMA (B3LYP/6-31+G(d,p) for S: 6-311++G(3df,3pd) in DMF). .	86
Table A.8.	Optimized ground state geometries of TX-S-AA _{endo} radical attack to MMA (B3LYP/6-31+G(d,p) for S: 6-311++G(3df,3pd) in DMF). .	87
Table A.9.	Optimized ground state geometries of PHC _{exo} radical attack to MMA (B3LYP/6-31+G(d,p) for S: 6-311++G(3df,3pd) in DMF). .	88
Table A.10.	Optimized ground state geometries of PHN _{exo} radical attack to MMA (B3LYP/6-31+G(d,p) for S: 6-311++G(3df,3pd) in DMF). .	89
Table A.11.	Optimized ground state geometries of PHO _{exo} radical attack to MMA (B3LYP/6-31+G(d,p) for S: 6-311++G(3df,3pd) in DMF). .	90
Table A.12.	Optimized ground state geometries of PHS _{exo} radical attack to MMA (B3LYP/6-31+G(d,p) for S: 6-311++G(3df,3pd) in DMF).	91
Table A.13.	Optimized ground state geometries of TX _{endo} radical attack to MMA (B3LYP/6-31+G(d,p) for S: 6-311++G(3df,3pd) in DMF).	92

LIST OF SYMBOLS

c	Molar concentration
E_{el}	Electronic energy
$E_c[\rho]$	Correlation energy
$E_x[\rho]$	Exchange energy
f_k^+	Fukui function of nucleophilic attack
f_k^-	Fukui function of electrophilic attack
f_k^0	Fukui function of radical attack
h	Planck's constant
h_{KS}	Kohn-Sham Hamiltonian operator
H	Hamiltonian operator
$I_0(\lambda)$	Intensity of used radiation
$I_a(\lambda)$	Absorbed radiation intensity
$J[\rho(r)]$	Coulomb energy
k	Reaction rate constant
k_B	Boltzmann's constant
l	Path length of radiation
S_n	Singlet excited states
T_n	Triplet excited states
$T[\rho(r)]$	Kinetic energy of interacting electrons
$T_{ni}[\rho(r)]$	Kinetic energy of non-interacting electrons
v	Imaginary frequency
$V_{ext}(r)$	External potential
$V_{ee}[\rho(r)]$	Electron-electron interactions
Z	Atomic number
δ	Diagonal matrix
ΔG^\ddagger	Gibbs free energy of activation
ΔG_{rxn}^o	Overall reaction Gibbs free energy

ΔH_{rxn}°	Overall reaction enthalpy
ϵ	Molar extinction coefficient
∇^2	Laplacian operator
ρ	Electron density
ψ_i	Kohn-Sham orbitals
Φ	Quantum yield
ϕ_S	Quantitative topological descriptor
Γ	Detachment density matrix
Λ	Attachment density matrix
Ψ	Wavefunction

LIST OF ACRONYMS/ABBREVIATIONS

B3LYP	Becke-3-Parameter Lee-Yang-Par Functional
B3LYP-D3	Becke-3-Parameter Lee-Yang-Par Functional with Dispersion Correction
DFT	Density Functional Theory
DMF	<i>N, N'</i> -Dimethylformamide
FRP	Free Radical Polymerization
GGA	Generalized Gradient Approximation
GTO	Gaussian Type Orbital
HF	Hartree-Fock Theory
HOMO	Highest Occupied Molecular Orbital
IC	Internal Conversion
IRC	Intrinsic Reaction Coordinate
ISC	Intersystem Crossing
LC	Long-Range Corrected
LCAO	Linear Combination of Atomic Orbitals
LDA	Local Density Approximation
LUMO	Lowest Unoccupied Molecular Orbital
M06-2X	Hybrid Meta Exchange-Correlation Functional
MMA	Methyl Methacrylate
NIR	Near Infrared Region
NPA	Natural Population Analysis
NTO	Natural Transition Orbital
oNTO	Occupied Natural Transition Orbital
PCM	Polarizable Continuum Model
PES	Potential Energy Surface
PHC	2-Phenylacetic Acid
PHC _{exo}	PHC Based Exocyclic Radical
PHN	<i>N</i> -Phenylglycine
PHN _{exo}	PHN Based Exocyclic Radical

PHO	2-Phenoxyacetic Acid
PHO _{exo}	PHO Based Exocyclic Radical
PHS	2-(Phenylthio)acetic Acid
PHS _{exo}	PHS Based Exocyclic Radical
POSS	Polyhedral Oligomeric Silsesquioxanes
PRC	Pre-Reactive Complex
STO	Slater Type Orbital
TADF	Thermally Activated Delayed Fluorescence
TD-DFT	Time Dependent Density Functional Theory
TS	Transition State
TX	Thioxanthone
TX _{endo}	TX Based Endocyclic Radical
TX-AA	2-(9-oxo-9H-thioxanthen-2-yl)acetic Acid
TX-AA _{endo}	TX-AA Based Endocyclic Radical
TX-AA _{exo}	TX-AA Based Exocyclic Radical
TX-NH-AA	(9-oxo-9H-thioxanthen-2-yl)glycine
TX-NH-AA _{endo}	TX-NH-AA Based Endocyclic Radical
TX-NH-AA _{exo}	TX-NH-AA Based Exocyclic Radical
TX-O-AA	2-((9-oxo-9H-thioxanthen-2-yl)oxy)acetic Acid
TX-O-AA _{endo}	TX-O-AA Based Endocyclic Radical
TX-O-AA _{exo}	TX-O-AA Based Exocyclic Radical
TX-S-AA	2-((9-oxo-9H-thioxanthen-2-yl)thio)acetic Acid
TX-S-AA _{endo}	TX-S-AA Based Endocyclic Radical
TX-S-AA _{exo}	TX-S-AA Based Exocyclic Radical
TX-SH	2-Mercaptothioxanthone
UV	Ultraviolet
UV-Vis	Ultraviolet Visible
vNTO	Virtual Natural Transition Orbital
XC	Exchange-Correlation
ω B97xD	Long-Range Corrected Hybrid Functional with Dispersion Correction

1. INTRODUCTION

Computational chemistry is a powerful way of investigating and characterizing chemical, physical and photophysical properties of reactions and novel compounds. Computational tools can be applied to elucidate the underlying factors of reactions, behaviors of compounds in different environments and propose a reaction mechanism. Different research groups have applied computational tools to investigate different properties of systems such as; structure-reactivity relationship [1], role of chain transfer agents [2], effect of substituents [3], solvent effect [4], reactivity studies [5, 6], kinetic studies [7], regioselectivity studies [8], and free radical polymerization [9].

Recent studies on photoinitiators focus on introducing new functionalities to both polymeric and monomeric photoinitiators to provide them with high absorptivity in spectral region of lamp emission, high photo-reactivity, high quantum yield, low or no toxicity, no odor, good solubility in the formulation and good shelf-life [10, 11]. Based on these reasons, understanding the physical, chemical, photophysical, kinetic and thermodynamic properties of photoinitiators has a crucial impact for providing detailed information on novel photoinitiators.

1.1. Photochemistry

Photochemistry can be defined as the study of photochemical reactions in which the reactions of light and the molecules are considered. Photochemical reactions require a photon to be absorbed to initiate the reactions. Photochemical reactions differ from thermal reactions. The activation of the photoreaction is based on the absorption of light whereas the activation of a thermal reaction is based on heat. For this reason, the electronic and nuclear configurations of molecules are different in photo activated molecules than the thermally activated molecules. One of the main advantages of light induced activation is to have a possibility to initiate the reaction at low temperatures. Photochemical reactions are favored when photons are absorbed by reactive molecules, namely the photoinitiators. After irradiation by a light source and photon absorption,

the light absorbing species are elevated to the higher energy levels and when they return to the lower energy levels the released energy may be transferred to generate species which have tendency to be reactive to surrounding molecules [12–20].

Photon absorption of a molecule, transforms the light energy into electronic excitation energy. The range of electromagnetic radiation is between the gamma rays to radio frequency waves (Figure 1.1 [12]). Generally, researchers have interest in the region of 200-1000 nm which includes the ultraviolet (UV) light (200-380 nm), visible region (at 380-760 nm) and the near-infrared (NIR) at 760-1000 nm for the photochemical reactions. It should be also mentioned that the difference in the wavelengths lead to difference in the penetration depths of the light. For this reason, the choice of wavelength is an important factor to be considered in the design of photochemical reactions. As an example, we can give the applications in radiation oncology. In radiation oncology, the target molecules are in a dense tissue of human body. The wavelength of the light source could be chosen accordingly for the penetration of light thorough this dense media to reach the photo-sensitive molecule for the activation [12–20].

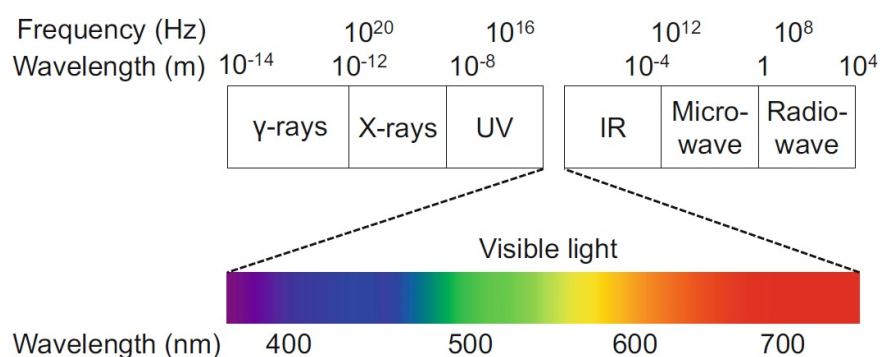


Figure 1.1. Electromagnetic spectrum and its regions.

1.1.1. Jablonski Diagram and Electronic Transitions

The Jablonski diagram (Figure 1.2) is used to describe the relative positions of the electronic and vibrational levels schematically. This representation is a useful way for the organization of the electronic structures, dynamic transitions and the electronic

energies of photophysical processes. The energy diagram shows the relative energies in the ground state, singlet excited states (S_n) and the triplet excited states (T_n) of a molecule [12–20].

Main transitions can be defined as:

- Singlet-singlet absorption ($S_0 + h\nu \rightarrow S_n$)
- Singlet-triplet absorption ($S_0 + h\nu \rightarrow T_n$)
- Singlet-singlet emission (Fluorescence) ($S_1 \rightarrow S_0 + h\nu$)
- Triplet-singlet emission (Phosphorescence) ($T_1 \rightarrow S_0 + h\nu$)
- Allowed transitions within same spin states (spin-allowed)
- Forbidden transitions of excited states in different spin states (spin-forbidden)

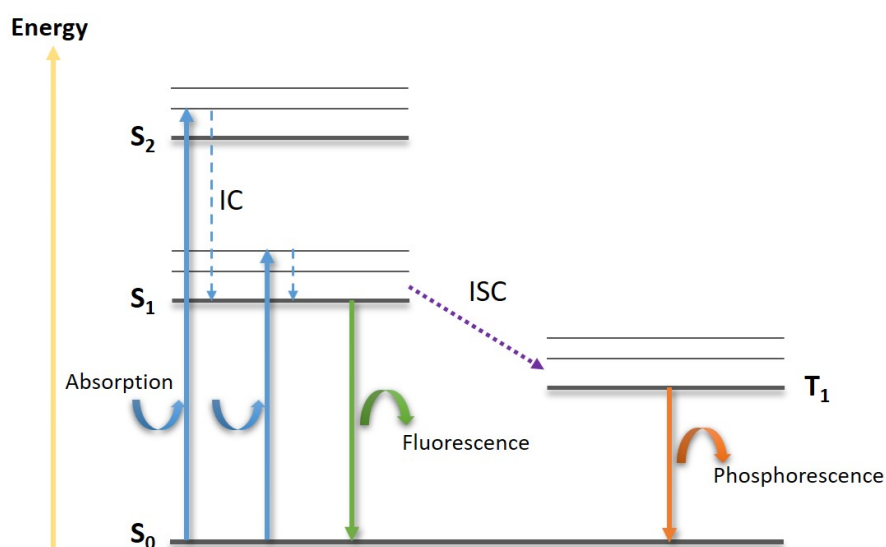


Figure 1.2. Jablonski diagram.

After absorption of the light, internal conversion can be observed. Internal conversion (IC) is a decay process where an excited molecule changes its state in same spin without radiation emission. In contrast, intersystem crossing (ISC) is a non-radiative transition between two different states accompanied by a change in the spin. Fluorescence is a radiative emission from the S_1 to S_0 , whereas the phosphorescence is a radiative emission from the T_1 to S_0 [12–16].

Absorption and emission spectra of photoreactive and sensitive molecules are often used in photochemical analysis of electronic transitions. As widely known, typical organic chromophores and luminophores have similar functional groups such as aromatic groups (benzene and fused ring structures), carbonyl group, vinyl group and nitroso group. Chromophores can be defined as atoms or functional groups that are responsible for the absorption and the color properties of the molecule whereas luminophores are responsible for the luminescent properties of the molecules, i.e. fluorescence and phosphorescence. Both of them can be organic or inorganic groups [12–20].

Table 1.1. Electronic transition types, their selection rules and corresponding absorption strengths of carbonyl group.

Transitions	Selection Rule	Absorption Strength
$\pi - \pi^*$	Allowed	Strong
$n - \sigma^*$	Symmetry forbidden	Weak
$n - \pi^* (S_0 \rightarrow S_n)$	Symmetry forbidden	Weak
$n - \pi^* (S_0 \rightarrow T_n)$	Symmetry and spin forbidden	Very weak

Electronic transitions can take place from bonding/non-bonding orbitals to anti-bonding orbitals that includes $\sigma - \sigma^*$, $\pi - \pi^*$, $n - \sigma^*$ and $n - \pi^*$ transitions. $\sigma - \sigma^*$ transition requires the highest energy to occur and the corresponding molecules exhibit radiation < 200 nm. Different transitions and their effects are dependent on the electron orbital configurations. For example, in the UV region of electromagnetic spectrum; two $n - \pi^*$ transitions take place for the carbonyl group (Table 1.1) [12]. These differ from each other by one being the triplet state and the other singlet state. As seen in Figure 1.2 the energy of triplet state is lower than the energy of the singlet state. For this reason, the absorption band in the triplet state possesses a longer wavelength. It should also be noted that the difference in the intensity of the absorption peaks are also related with the selection rules. $\pi - \pi^*$ transitions, completely allowed transitions, show a high absorption maximum compared to the symmetry forbidden transitions, $n - \pi^*$.

1.2. Photoinitiators

Photoinitiators are the molecules that are sensitive to light. After irradiated by a light source they are capable of reaching different excited states and use this energy to form reactive species, mostly the radicals. Photoinitiators are the key components of the photoinitiated free radical polymerization. Their molecular design is directly linked to their capabilities and efficiencies as a photoinitiator. Main role of the photoinitiator is the conversion of the radiation energy, obtained from a light source, into a useful form for chemical processes [12–18].

The performance of a photoinitiator in the initiation process is dependent on many factors. However, these factors can be summarized as; the efficiency of the radiation absorption, efficiency of radical generation and the reactivity and life time of the generated radicals [21].

An indicator for the absorption efficiency is the Quantum Yield (Φ) [12–18]. The maximum value of Φ can be 1 and this means that for each absorbed photon one photon is emitted (Equation 1.1).

$$\Phi = \frac{\text{Number of photons emitted}}{\text{Number of photons absorbed}} \quad (1.1)$$

Φ can be used for the calculation of some kinetic properties such as the rate of the radical formation process. The rate of radical formation step (R_i), at a wavelength (λ) can be calculated by:

$$R_i = \Phi_i \cdot I_a(\lambda) = \Phi_i \cdot I_0(\lambda) \cdot (1 - e^{-2.3 \cdot \epsilon(\lambda) \cdot l \cdot c}) \quad (1.2)$$

in which the Φ_i represents the quantum yield of radical formation step, $I_a(\lambda)$ is the radiation intensity that photoinitiator absorbs. If the photoinitiator is the only light-absorbing specie, $I_a(\lambda)$ can be calculated by Lambert-Beer equation. $I_0(\lambda)$ represents the intensity of the used radiation, $\epsilon(\lambda)$ is the molar extinction coefficient (stands for the absorbance of the photoinitiator), c is the molar concentration of the photoinitiator,

and l is the path length of the radiation. As it can be seen in the Equation 1.2, $\epsilon(\lambda)$ and $I_0(\lambda)$ are related with the wavelength of the light source. For this reason, in the case of polychromatic light source usage, the total rate of the radical formation step can be calculated as the integral of the Equation 1.2 over the range of generated wavelength of the light source [12, 17].

Photopolymerization has a great interest in polymer science and technology due to its wide variety of applications such as UV-curing, coatings, adhesives, inks, dental materials, 3D-printing, biomedical and biochemical applications [10, 11, 22–25]. Upon irradiation of photoinitiators, the following reactions may occur;

- (i) fragmentation by photocleavage of the bonds,
- (ii) transfer of its energy to another molecule to form radicals which initiate the polymerization,
- (iii) abstraction of hydrogen from another molecule and thus creating a radical which will initiate the reaction.

According to these reactions, photoinitiators can be classified in 3 main categories [12–19]:

- (i) *Type I* Photoinitiators
- (ii) *Type II* Photoinitiators
- (iii) *One-Component Type II* Photoinitiators

Photoinitiators that form radicals by photo-fragmentation are called *Type I* and photoinitiators that form radicals by hydrogen abstraction are called *Type II* photoinitiators. *Type II* photoinitiators need a synergist / co-initiator to form radicals and the radicals that are responsible for the initiation of the polymerization are formed on the co-initiator molecule. On the other hand, there is another type of photoinitiator which can be classified as *One-Component Type II* photoinitiator. This type of photoinitiator does not require a co-initiator and is capable of making intermolecular or intramolecular hydrogen abstraction. Therefore, radical species responsible for the initiation of

the polymerization are formed on the photoinitiator and the reaction proceeds from these radicals [11, 26, 27]. Each type of photoinitiator shows different photochemical and photophysical properties in photoinitiated free radical polymerization reactions. The following subsections are dedicated to the more detailed information on the types of photoinitiators.

1.2.1. *Type I* Photoinitiators

In this class, most of the photoinitiators are based on substituted acetophenone structure. This type of photoinitiator undergoes a homolytic bond cleavage (α or β cleavage) upon irradiation by a light source and forms two corresponding radicals. This mechanism is also called as *Norrish Type I* reaction. General reaction of a *Type I* system is given in Figure 1.3. [10, 17, 27].

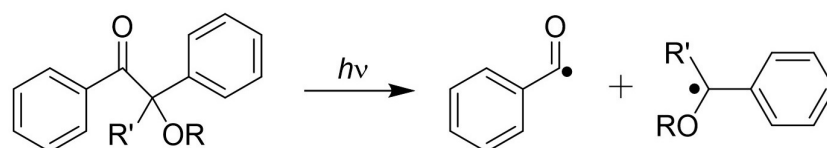


Figure 1.3. *Type I* radical formation reaction.

R and R' can be hydrogen, alkyl or substituted alkyl. Both of the formed radicals have capability of initiating the polymerization with slightly different efficiency. Their molecule structure and radical properties, such as spin density, are effective on their initiating capabilities [21].

Most versatile photoinitiators of this class are α -hydroxyketones (Figure 1.4). These compounds provide high efficiency, good shelf-life and almost no yellowing of the synthesized products. α -hydroxyketones can be modified with chromophoric substituents such as benzene rings and carbonyl containing groups to gain efficient light absorption characteristics.

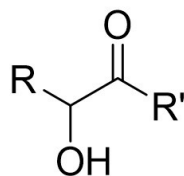


Figure 1.4. Structure of α -hydroxyketone.

Widely known example of *Type I* photoinitiators is a commercial photoinitiator family called *Irgacure*. Irgacure family have variety of different molecule structures according to their chemical class and they are denoted by numbers, i.e. Irgacure 2959. Irgacure 2959 belongs to the chemical class of α -hydroxyketone. The unimolecular *Type I* radical formation reaction of Irgacure 2959 is given in Figure 1.5 for a better understanding of the *Type I* radical formation [21,28].

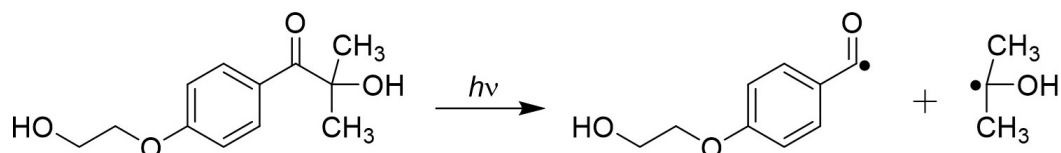


Figure 1.5. *Type I* radical formation reaction of Irgacure 2959.

1.2.2. *Type II* Photoinitiators

As previously mentioned, *Type II* systems are bimolecular systems which require an extra compound in the reaction media for the radical formation. These extra compounds are called co-initiators/synergists. Formation of the initiating species (radicals) may occur through an electron transfer reaction, hydrogen abstraction or within a combined process of both the electron transfer and hydrogen abstraction. This route is mainly dependent on the nature of the photoinitiator and the co-initiator. *Type II* photoinitiators are generally benzophenone, xanthone or thioxanthone based molecules (Figure 1.6) [10, 17, 21, 27].

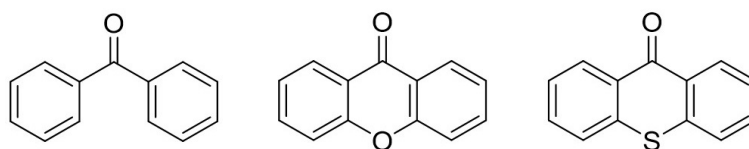


Figure 1.6. Structures of benzophenone, xanthone and thioxanthone.

For the *Type II* reaction of thioxanthone; in the presence of a hydrogen donor co-initiator, i.e. amines, electron transfer between the triplet state thioxanthone (acting as an acceptor) and the co-initiator (acting as a donor) may form an ion pair intermediate (a TX radical anion and a donor radical cation) excited state complex, called exciplex. Thus, a proton transfer from the α position of the co-initiator to the TX results in a ketyl radical on the photoinitiator and another radical on the co-initiator. However, direct abstraction of hydrogen is also possible when alcohols, ethers, carboxylic acids are used as the co-initiators [10, 17, 21, 27].

Because of the resonance stabilization and steric effects, the ketyl radicals on thioxanthone molecules are assumed to have no effect for the initiation of the polymerization. They are assumed to be participating in the combination or in the termination of the polymer chains. On the other hand, radicals which are formed on the co-initiator compounds are efficient for the initiation of the polymerization. General reaction of the radical formation of thioxanthone is given in Figure 1.7 where the R-H is the hydrogen donor (co-initiator) [27].

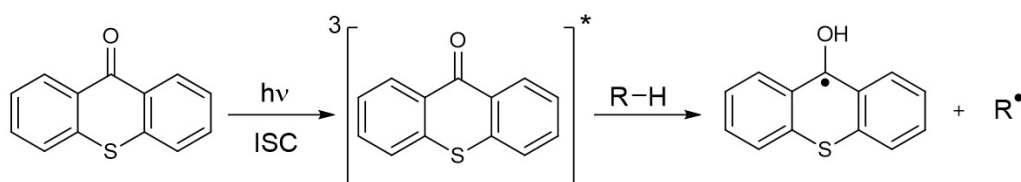


Figure 1.7. *Type II* radical formation reaction of thioxanthone.

It is known that heteroatom containing co-initiators are efficient for the promotion of radical formation, but the most efficient co-initiators belong to the class of tertiary amines which have strong hydrogen donation capabilities. Mostly used co-initiators are derived from the amines, thiols, alcohols, ethers, silanes etc. Some of the mostly used co-initiator structures are given in Figure 1.8 [27].

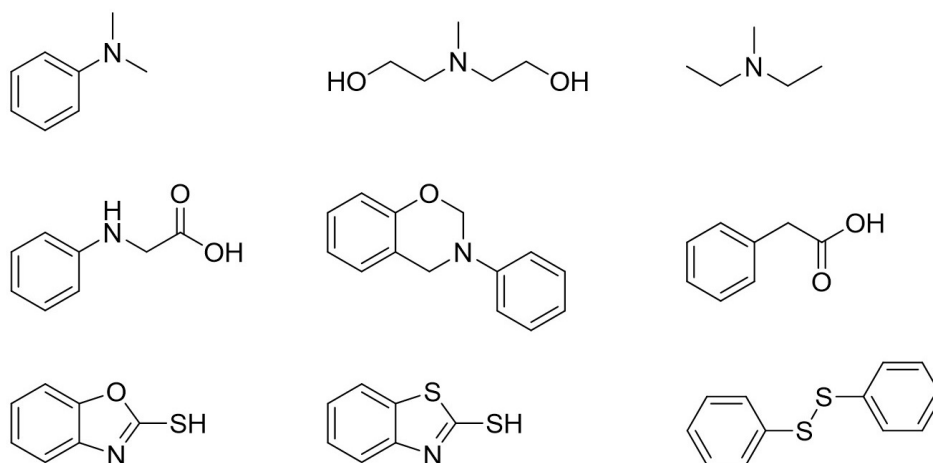


Figure 1.8. Examples of co-initiators in *Type II* reactions.

1.2.3. *One-Component Type II* Photoinitiators

The research focuses on *Type II* photoinitiation systems to design novel photoinitiators that have the capability of being the photoinitiator and the co-initiator at the same time. The main approach is the incorporative synthesis of the photoinitiators by adding co-initiators into the photoinitiator structures. Thus, the novel molecules can exhibit double functionality. The main advantage of *One-Component* systems is to have no need for an additional molecule in the system to initiate the polymerization. Initiating species can be formed through intermolecular or intramolecular interactions between the triplet state chromophore core and the co-initiator part of the photoinitiator molecule. Some disadvantages of using individual co-initiators such as strong odor, yellowing and ease of purification of the polymer can be solved by the usage of *One-Component* systems.

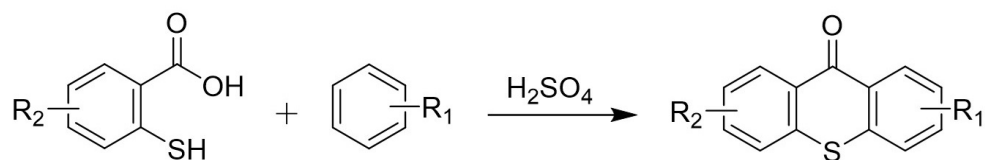


Figure 1.9. Synthesis of thioxanthone and its derivatives.

For this reason, amine, thiol, ether, carboxylic acid and other molecules which have hydrogen donor capability have been incorporated into the photoinitiator structures to design new *One-Component* photoinitiating systems. Figure 1.9 shows the synthesis of thioxanthone and thioxanthone derivatives by the condensation reaction of thiosalicylic acid and an aromatic compound in the presence of concentrated sulfuric acid [27]. R₁ and R₂ groups can be modified as the hydrogen donor/co-initiator and *One-Component* thioxanthone based *Type II* photoinitiators can be synthesized by this approach.

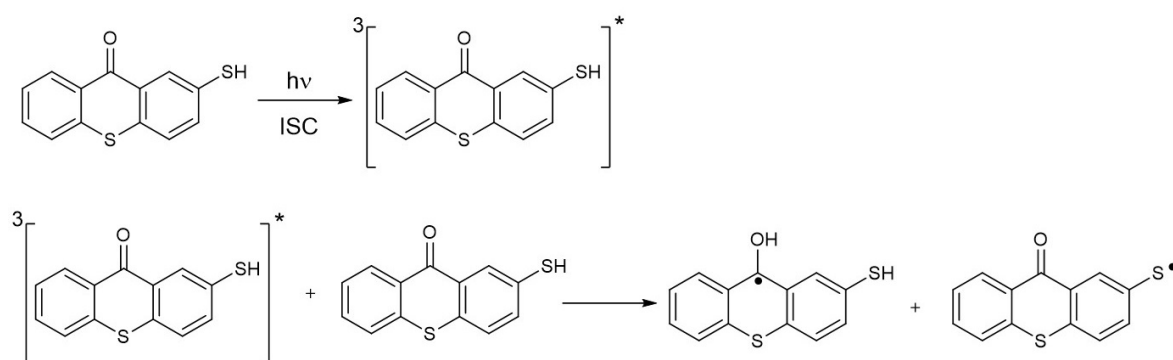


Figure 1.10. *One-Component Type II* radical formation reaction of TX-SH.

One of the previously reported thioxanthone based *One-Component Type II* photoinitiator is 2-mercaptothioxanthone (TX-SH). It is synthesized by reacting the thiosalicylic acid with thiophenol in a concentrated sulfuric acid media. The radical formation reaction is based on the intermolecular interaction between the triplet TX-SH and a ground state TX-SH molecule. This interaction result in the formation of thiyl radicals. Intramolecular interaction between the carbonyl and thiol group is unlikely

to occur since the bond between the thioxanthone core and thiol group is rigid. Therefore, the dominant reaction is through the intermolecular hydrogen abstraction (Figure 1.10) [10, 23, 27, 29].

1.2.4. Thioxanthenes as Photoinitiators

Thioxanthone and its derivatives are widely used as photoinitiators for photoinitiated polymerization. Their photopolymerization properties are deeply investigated by experimental methods [30–38] and it is known that thioxanthone can be functionalized to synthesize *One-Component Type II* photoinitiators [29]. Thioxanthone and thioxanthone based *One-Component Type II* photoinitiators are used in variety of studies and in different areas of interests; as photoinitiators [29, 35–38], as reduction agents for metal nanoparticle synthesis [24, 39], for DNA binding mode studies [40], for functionalizing polyhedral oligomeric silsesquioxane (POSS) structure [41], for nanocomposite preparations [39], and recently as candidates for thermally activated delayed fluorescence (TADF) emitters. [42–44].

Thioxanthone based molecules and some different photoinitiators, such as the mostly known industrial photoinitiator Irgacure, have been also investigated by computational tools such as DFT by different groups [45–48].

In this study, the initiation capabilities of four different thioxanthone based *One-Component Type II* photoinitiators are investigated [35–38]. Furthermore, phenyl acetic acid derivatives have also been studied to compare the advantages of *One-Component Type II* photoinitiators against *Type II* photoinitiators (Figure 1.11).

As mentioned earlier, capability of light absorption of a molecule plays a significant role to absorb and use the energy for radical formation. Thioxanthone acetic acid derivatives have more π electrons (bonding, non-bonding and anti-bonding), conjugation and more delocalization of electrons in the structure compared to the phenyl acetic acid derivatives (Figure 1.11). Thus, thioxanthone acetic acid derivatives are capable of more light absorption in a larger spectrum and at higher wavelengths.

The molecules considered in this study are given below:

(i) Thioxanthone acetic acid derivatives

- 2-(9-oxo-9H-thioxanthen-2-yl)acetic acid (TX-AA)
- (9-oxo-9H-thioxanthen-2-yl)glycine (TX-NH-AA)
- 2-((9-oxo-9H-thioxanthen-2-yl)oxy)acetic acid (TX-O-AA)
- 2-((9-oxo-9H-thioxanthen-2-yl)thio)acetic acid (TX-S-AA)

(ii) Phenyl acetic acid derivatives

- 2-phenylacetic acid (PHC)
- *N*-phenylglycine (PHN)
- 2-phenoxyacetic acid (PHO)
- 2-(phenylthio)acetic acid (PHS)

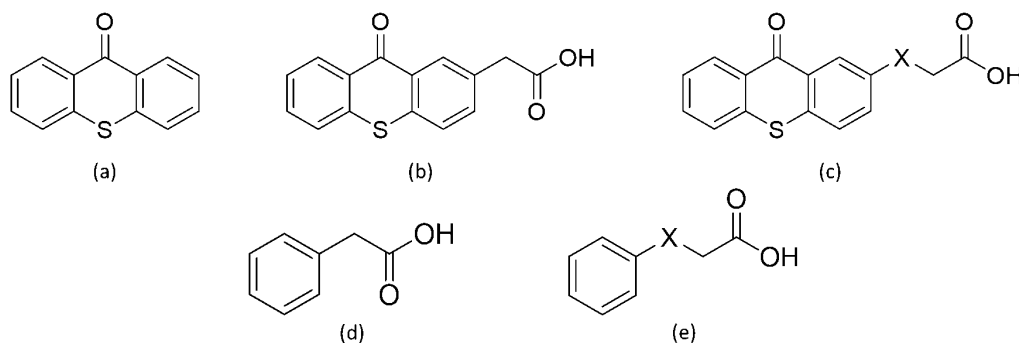


Figure 1.11. Molecule structures of thioxanthone and phenyl acetic acid derivatives.

In Figure 1.11 (a) represents thioxanthone, (b) represents TX-AA, (c) represents TX-NH-AA, TX-O-AA and TX-S-AA, (d) represents PHC, (e) represents PHN, PHO and PHS. NH group, oxygen (O) and sulfur (S) atoms are denoted by X in the molecule structures.

2. METHODOLOGY

Main focus in quantum chemistry is to solve the Schrödinger equation since the wavefunction parameter of the equation contains information related to the particle. For instance, Heisenberg Uncertainty Principle [49] states that the exact position and the momentum of a particle cannot be determined at the same time. Nevertheless, this can be overcome by the calculation of the probability of the positions of the particle by squaring the wavefunction which is obtained by solving the Schrödinger's equation:

$$H\psi = E\psi \quad (2.1)$$

in which H is the Hamiltonian Operator and provides the total energy of the system (E) as an eigenvalue and ψ in both sides represent the wavefunction. Since the H operator is composed of the potential and kinetic energy terms of the electrons and the nuclei, it can be defined as:

$$H = -\sum_i \frac{\hbar^2}{2m_e} \nabla_i^2 - \sum_k \frac{\hbar^2}{2m_k} \nabla_k^2 - \sum_i \sum_k \frac{e^2 Z_k}{r_{ik}} + \sum_{i<j} \frac{e^2}{r_{ij}} + \sum_{k<l} \frac{e^2 Z_k Z_l}{r_{kl}} \quad (2.2)$$

where all five components of the equation describe the energy of the system. The initial two terms represent the kinetic energy value of the electrons and the nuclei, respectively. These terms are followed representative terms of the potential energies as the result of Coulomb interactions of nucleus-electron, electron-electron and nucleus-nucleus. In the equation, electrons are represented by i and j , the nuclei as k and l , m_k and m_e are the masses of nuclei and electrons, respectively. \hbar stands for "h/2 π " where h is the Plank's constant, electron charge is denoted by e , atomic number is denoted by Z , the distance between the particles is denoted by r and the Laplacian operator is denoted by ∇^2 .

One can state that the Schrödinger equation can be accurately applied to small systems such as the hydrogen atom and the hydrogen-like ions, however the Schrödinger

equation cannot provide an exact solution for many-particle systems because of the interacted motions of particles. Since, the mass of nuclei are much higher than the electrons, they possess themselves as stationary charged points in the system compared to the electrons. For this reason, their kinetic energy terms would be zero. On the other hand, Born-Oppenheimer approximation [50] proposes to take into account the electronic and nuclear motions separately for the elimination of the nucleus-electron attraction term and taking the nuclear-nuclear repulsion term constant. After taking into consideration this approach, the Hamiltonian operator can be defined as:

$$H_{el} = E_k^{kin} + U_{ki} + U_{ij} \quad (2.3)$$

where U_{ki} is the potential energy of nucleus-nucleus and U_{ij} is the potential energy of electron-electron interactions. If we apply this approximation to the Schrödinger equation than we represent as:

$$(H_{el} + V_{nn})\psi_{el} = E_{el}\psi_{el} \quad (2.4)$$

where V_{nn} is the nucleus-nucleus repulsion energy constant, and the E_{el} is the electronic energy eigenvalue.

The rewritten Schrödinger equation (Equation 2.4) can be used for all other systems by using the variational principle. When we multiply the both sides of the Equation 2.1 with the term ψ , it becomes:

$$\psi H \psi = \psi E \psi \quad (2.5)$$

For many electron containing systems, integration of both sides in Equation 2.5 for a volume of $d\tau$ results in:

$$\omega = \frac{\int \psi H \psi d\tau}{\int \psi^2 d\tau} \quad (2.6)$$

where ω is the calculated energy value. According to this theorem, calculated energy value can only be equal or greater than the ground state energy (E_0). By this way, approximate solutions of the Schrödinger equation can be obtained.

In this study, mainly Density Functional Theory based methods, which is a variational method, are used.

2.1. Density Functional Theory

DFT [51] is a widely used quantum chemistry approach suggested by Hohenberg and Kohn in 1964 [52, 53]. The basis of the DFT are Kohn-Hohenberg Existence theorems [54]. These theorems allow the calculation of the electronic structure of molecules. According to first theorem of Kohn-Hohenberg, ground state densities of molecules are adequate to determine the wavefunction. The electron density can be written as in Equation 2.7 in which the coordinates of the electrons are denoted by r .

$$\rho(r) : N \int \dots \int |\Psi(r_1, r_2, \dots, r_n)|^2 dr_1 dr_2 \dots dr_n \quad (2.7)$$

Second theorem of Kohn-Hohenberg states that by the usage of variational principle, the ground state energy can be calculated since the ground state density is defined as the density which minimizes the total energy of the system [54]. Electronic energy of the ground state can be expressed as a function of the electron density as given below:

$$E[\rho(r)] = \int V(r)\rho(r)dr + T[\rho(r)] + V_{ee}[\rho(r)] \quad (2.8)$$

If the theorem developed by Kohn and Sham [55] is applied to the Equation 2.8 the electronic energy equation can be rewritten as:

$$E[\rho(r)] = \int V(r)\rho(r)d(r) + T_{ni}[\rho(r)] + J[\rho(r)] + E_{XC}[\rho(r)] \quad (2.9)$$

The terms in Equation 2.9 are; ($J[\rho]$) the Coulomb energy, ($T_{ni}[\rho]$) kinetic energy value of the non-interacting electrons, and ($E_{XC}[\rho]$) the exchange-correlation energy functional. In this representation of the Coulomb energy ($J[\rho]$), correlations between the motions of the electrons are not taken into account. The Coulomb energy of electron-electron interactions term can be written as:

$$J[\rho(r)] = - \sum_{A=1}^M \int \frac{Z_A}{|r - R_A|} \rho(r) dr + \int \frac{\rho(r_1)\rho(r_2)}{|r_1 - r_2|} dr_1 dr_2 \quad (2.10)$$

in which the M represents the total number of nuclei in the system. Moreover, the kinetic energy term which represents the measure of the freedom for non-interacting electrons can be written as:

$$T_{ni}[\rho(r)] = \sum_{i=1}^N \int \psi_i(r) - \frac{\nabla^2}{2} \psi_i(r) dr \quad (2.11)$$

where the denotation N represents the total number of the electrons. The last term of the Equation 2.9 is the exchange-correlation energy functional. It can be defined as the sum of an exchange functional ($E_X[\rho]$) and a correlation functional ($E_C[\rho]$) despite the fact that it has a correlation between the kinetic energy term which arises from the kinetic energy difference between the interacting and non-interaction electron systems [56]. The exchange-correlation energy is:

$$E_{XC}[\rho(r)] = \int \rho(r) \epsilon_{XC}(\rho(r)) dr \quad (2.12)$$

By the derivation of Equation 2.12 with electron density term, the equation can be rearranged as:

$$V_{XC}[\rho(r)] = \rho(r) \frac{d\epsilon_{XC}(\rho(r))}{d\rho(r)} + \epsilon_{XC}(\rho(r)) \quad (2.13)$$

In density functional theory of Kohn-Sham; independent orbitals, namely Kohn-Sham orbitals (ψ_i) are obtained by solving the Kohn-Sham equations.

$$h_{KS}\psi_i = \varepsilon_i\psi_i \quad (2.14)$$

where h_{KS} stands for the Kohn-Sham Hamiltonian operator. Kohn-Sham Hamiltonian operator is defined as:

$$h_{KS} = -\frac{\nabla^2}{2} - \sum_{A=1}^N \frac{Z_A}{|r - R_A|} + \int \frac{\rho(r_1)\rho(r_2)}{|r_1 - r_2|} dr_1 dr_2 + V_{XC}[\rho(r)] \quad (2.15)$$

$V_{XC}[\rho(r)]$ being the exchange correlation potential which is related with the exchange correlation energy defined in Equation 2.13. The Kohn-Sham orbitals are capable of giving the exact density if the exact form of the exchange correlation functional is known by the equation below:

$$\rho(r) = \sum_{i=1}^N |\psi_i|^2 \quad (2.16)$$

Regardless, the exact form of the exchange-correlation functional is not known. Different functionals represent the different approximations of this exchange-correlation functional. More detailed information about the functionals are given in the following section.

2.2. Functionals

In parallel with the development of DFT, variety of approximations have been developed with a focus of determination of the exact form of the exchange-correlation functional. The first approximation is the Local Density Approximation (LDA) which is the root of the exchange-correlation functionals. LDA provides the uniform electron gas energy and treats the electron density of the system as equal in each site. The positive charge accompanies to make the system neutral.

The energy expression is given below:

$$E[\rho] = T_{ni}[\rho] + \int \rho(r)v(r)dr + J[\rho] + E_{xc}[\rho] + E_b \quad (2.17)$$

where E_b is defined as the electrostatic energy of the positivity. Since the electron and positive charge densities are known to be equal, the Equation 2.17 can be minimized to:

$$E[\rho] = T_{ni}[\rho] + E_{xc}[\rho] \quad (2.18)$$

and the E_{xc} parameter can be divided into two individual parts (i) an exchange functional and (ii) a correlation functional. Thus, the equation can be reorganized by replacement of the E_{xc} term within these newly established functionals as:

$$E[\rho] = T_{ni}[\rho] + E_x[\rho] + E_c[\rho] \quad (2.19)$$

Further, the kinetic energy functional is:

$$T_{ni}[\rho] = C_F \int \rho(r)^{5/3} dr \quad (2.20)$$

with C_F being constant and equal to 2.8712. The exchange functional can be defined by the following equation:

$$E_x[\rho] = -C_x \int \rho(r)^{4/3} dr \quad (2.21)$$

with C_x being constant and equal to 0.7386. $E_c[\rho]$ is the correlation energy term for uniformly distributed electron gas which is obtained by the parametrization of the results that are generated by a set of quantum Monte Carlo calculations. But, LDA is not adequate to determine the exact form of the exchange-correlation functional. Uniform distribution of the electron density is not possible since the electron densities differ in a molecule.

Generalized Gradient Approximation (GGA) [57] takes into account the heterogeneous nature of electron density by the postulation of the exchange and the correlating energies dependent not only the density, as well as on its gradient. The expression of the energy by GGA is defined as:

$$E_{XC}^{GGA}[n] = \int dr n(r) \epsilon_{XC}(n(r), |\nabla n(r)|) \quad (2.22)$$

As an example of an alternative approach can be given as the hybrid density functional methods which are the combination of the GGA method with a percentage of Hartree-Fock (HF) exchange. These functionals are capable of adding the exact exchange, calculated by HF functional, to the DFT exchange and correlation. Mostly known example is the B3LYP [52, 58]. B3LYP has the form of a mixed LDA and GGA functionals as described below:

$$E_{XC}^{B3LYP} = (1 - a)E_X^{LSDA} + aE_X^{HF} + b\Delta E_X^B + (1 - c)E_C^{LSDA} + cE_C^{LYP} \quad (2.23)$$

in which the empirical coefficients are defined as 0.20, 0.72 and 0.81, respectively [59].

Another well-known hybrid density functional example is; M06-2X (Equation 2.24), which is a member of Minnesota Functional family that is developed by the team of Prof. Donald Truhlar [60]. The hybrid exchange correlation for M06-2X can be written as:

$$E_{XC}^{hyb} = \frac{X}{100} E_X^{HF} + (1 - \frac{X}{100}) E_X^{DFT} + E_C^{DFT} \quad (2.24)$$

where X denotes the percentage of Hartree-Fock exchange, and equals to 54 for the M06-2X functional.

One of the other approaches to be mentioned is the long-range corrected (LC) hybrid density functionals which have 100% HF exchange for long-range electron-electron interactions.

The long-range corrected hybrid density functional approximation (LCDFA) can be described as:

$$E_{XC}^{LCDFA} = E_X^{SR-DFA}(\omega) + E_X^{LR-HF}(\omega) + E_C^{DFA} \quad (2.25)$$

Mostly known example for LC hybrid density functional is; ω B97XD [61], which has only a small fraction for short-range exact exchange around 22% and 100% for long-range exact exchange. The long-range correction provides beneficial improvement for some features such as; charge transfer excitations, optical properties, long-chain polarizability and dissociation of two-centered three electron bonds [62].

2.3. Basis Sets

Basis set term is first described by John C. Slater as the orbitals within a system as a set of functions [63]. Generally, basis functions are expanded in terms of a linear combination of atomic orbitals, also known as LCAO, with various coefficients.

$$\phi_i = \sum_{\mu=1}^K c_{\mu i} f_{\mu} \quad (2.26)$$

where the functions μ_i represents molecular orbitals, f_{μ} atomic orbitals, $c_{\mu i}$ are coefficients and K is the total number of atomic orbital functions, which are also basis functions.

Basis sets are composed of mainly 2 classes; Slater-type orbitals (STOs) and Gaussian-type orbitals (GTOs). STOs are accurate to provide a solution for the Schrödinger equation for hydrogen atoms but their computational cost is high. Contrarily, GTOs are preferable over STOs since the increase in the number of integrals brings an increase of the computational time. S. Francis Boys [64] introduced GTOs in 1950 and ever since they are widely employed basis sets in DFT studies. They can also be defined as the approximated-analogues of the STOs.

Pople *et al.* developed the split-valence basis sets by treating the core and valence orbitals differently. Overall, one basis functional is applied to each core atomic orbitals and a larger basis is employed for the valence atomic orbitals. Since the core electrons are known to be less effected by the chemical environment compared to the valence electrons, valence electrons are treated with larger basis set while the core electrons are treated with a minimal basis set. Mostly known examples of the split-valence basis sets are; 3-21G, 6-21G, 6-31G*, 6-311G**, 6-31++G** and 6-31+G**. More examples of Pople basis sets are present in the literature.

Polarization functions can be included in basis sets in order to improve the basis set flexibility for the system to conclude mathematical calculations and to represent the system better.

The usage of appropriate functionals and basis sets in a quantum mechanical calculation is very essential. An increase in the complexity of basis sets leads to an increase in the accuracy of the calculation but in the same time the computational cost. For this reason, basis sets should be chosen according to the necessities of the accuracy level together with a reasonable computational cost.

2.4. Time-Dependent Density Functional Theory

TD-DFT is a tool that is used for the calculation of electronic excited properties of a system. TD-DFT is based on the Runge-Gross theorem [65]. It is a time-dependent analogue of Kohn-Hohenberg theorem. By this approach, the Hamiltonian operator can be written as:

$$\hat{H} = \hat{T}(r) + \hat{W}(r) + \hat{V}_{ext}(r, t) \quad (2.27)$$

in which the $\hat{T}(r)$ is the kinetic energy of electrons, $\hat{W}(r)$ is the Coulomb interaction between the electrons and the last term, $\hat{V}_{ext}(r, t)$, is the time-dependent potential effect on electrons.

The excited state energy is mostly dependent on the external potential. For this reason, determination of the potential effects on the system is a necessity to calculate the excited state properties. The Kohn-Hohenberg theorem can be applied to the variational principle as below:

$$A = \int_{t_0}^{t_1} \langle \Psi(t) | i \frac{\partial}{\partial t} - \hat{H} | \Psi(t) \rangle dt \quad (2.28)$$

and the wavefunction is defined as a time-dependent constant:

$$\Psi(r_1, \dots, r_N, t) = \Psi[\rho](t) e^{-ia(t)} \quad (2.29)$$

The phase factor adds a constant in Equation 2.29:

$$A[\rho] = \int_{t_0}^{t_1} \langle \Psi(t) | i \frac{\partial}{\partial t} - \hat{H}(t) | \tilde{\Psi}[\rho](t) \rangle dt + a(t_1) - a(t_0) = A[\rho] + \text{const.} \quad (2.30)$$

$A[\rho]$ can be reorganized as:

$$A[\rho] = B[\rho] - \int dr \int_{t_0}^{t_1} (r, t) \rho(r, t) dtv \quad (2.31)$$

where $B[\rho]$ stands for the independence of the external potential. By assuming that independent system has the property which can be described as:

$$\rho(r, t) = \sum_i f_i |\Psi(r, t)|^2 \quad (2.32)$$

$B[\rho]$ can be reorganized as:

$$B[\rho] = \sum_i f_i \int_{t_0}^{t_1} \langle \Psi_i(t) | i \frac{\partial}{\partial t} - \frac{1}{2} \nabla_i^2 | \psi_i(t) \rangle dtv - \frac{1}{2} \int_{t_0}^{t_1} dt \iint dr_1 dr_2 \frac{\rho(r_1, t) \rho(r_2, t)}{|r_1 - r_2|} - A_{XC}[\rho] \quad (2.33)$$

where $A_{XC}[\rho]$ is the exchange and correlation action functional.

Application of the variational principle to Equation 2.31 with constraints leads to:

$$\rho(r, t) = \sum_i f_i |\Psi_i(r, t)|^2 = \sum_i^N |\Psi_i(r, t)|^2 \quad (2.34)$$

Time-dependent Kohn-Sham equation is:

$$\left[-\frac{1}{2}\nabla^2 + v_{eff}(r, t)\right]\Psi_i(r, t) = i\frac{\partial}{\partial t}\Psi_i(r, t) \quad (2.35)$$

$$v_{eff}(r, t) = v_H(r, t) + v_{xc}(r, t) + v_{ext}(r, t) \quad (2.36)$$

where the time-dependent exchange potential is the unknown. All exchange and correlation effects are collected in Equation 2.37:

$$v_{xc}(r, t) = \frac{\delta A_{xc}[\rho]}{\delta \rho(r, t)} \quad (2.37)$$

Even though the equations in TD-DFT are exact with no approximations; in order to determine the unknown part, functional of the exchange-correlation, adiabatic approximation (AA) is applied:

$$v_{xc}[\rho](r, t) = \frac{\delta A_{xc}[\rho]}{\delta \rho(r, t)} \approx \left. \frac{\delta E_{xc}[\rho]}{\delta \rho(r)} \right|_{\rho=\rho(r, t)} \quad (2.38)$$

The exchange and correlation potential changes instantly when/if the electron densities change.

2.5. Polarizable Continuum Model

During the quantum mechanical calculations, solvation models are used to mimic the solvent environment in order to gain more realistic results of the system.

Solvent models can be applied either implicitly and/or explicitly (Figure 2.1). In explicit solvation models, the solvent molecules are added to the model separately. The implicit solvent model is generally used as compared to the explicit solvent model in which the solvation is described as a solvent continuum.

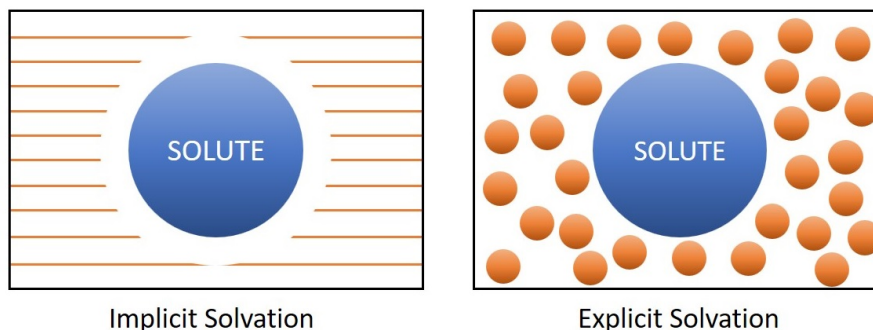


Figure 2.1. Illustration of implicit and explicit solvation models.

Implicit solvation model is the most effective way to include condensed phase effects to the calculations. The implicit solvent model is also called as continuum solvation model where different physical effects are included for the overall solvation process. The total solvation free energy can be expressed as:

$$\Delta G_{\text{solvation}} = \Delta G_{\text{cavity}} + \Delta G_{\text{dispersion}} + \Delta G_{\text{electrostatic}} + \Delta G_{\text{repulsion}} \quad (2.39)$$

where ΔG_{cavity} is the energy of solute addition to the system environment. $\Delta G_{\text{dispersion}}$ is the interaction energy between the solvent and the solute. This term adds the stabilization to solvent free energy. Solute-solvent electrostatic interactions energy is denoted by $\Delta G_{\text{electrostatic}}$. $\Delta G_{\text{repulsion}}$ is the exchange solute-solvent interactions which are not included in the ΔG_{cavity} . All terms are calculated by the usage of a defined cavity through van der Waals spheres which are centered at the atomic positions.

One of the polarizable continuum solvation models is the Polarizable Continuum Model (PCM) which was developed by Tomasi *et al.* [66]. In PCM, the cavity is formed by a set of spheres that are centered on atoms. These spheres have radii identified by

the multiplication of the van der Waals radii of the atoms by a constant factor. The solute is embedded into this identified cavity. Afterwards, subdivision of the cavity creates small domains and the polarization charges are embedded into these small domains. PCM considers that the solvent has only a single and specifically defined dielectric constant with the assumption of the charge distribution of the solute induces a polarization.

PCM can be classified into 3 main approaches; Dielectric PCM (D-PCM), which is the first formulation of PCM, Conductor-like PCM (C-PCM) and the Integral Equation Formalism of the PCM (IEF-PCM). C-PCM provides the solvation in terms of a surrounding medium modelled as a conductor instead of a dielectric. IEF-PCM is an implementation of reformed PCM equations.

2.6. Wigner Distribution Function

The Wigner distribution function was first proposed by E. Wigner as a set of quantum corrections to classical mechanics [67]. The Wigner quasi-probability distribution, also called as the Wigner-Ville Distribution, was proposed in order to associate the wavefunction and the probability distribution in phase space. As a result, combined distribution of the momentum and the particle positions are described in terms of the wavefunction (Ψ).

By the usage of either the coordinate-space or the momentum-space, the Wigner distribution ($W(x, p)$) can be obtained. For one-dimensional system, the Wigner transform (by using the coordinate-space wavefunction) can be written as:

$$W(x, p) = \frac{1}{2\pi} \int_{-\infty}^{\infty} \psi^*\left(x + \frac{s}{2}\right) \psi\left(x - \frac{s}{2}\right) e^{ips} ds \quad (2.40)$$

in which ψ is the wavefunction, x is the position and p is the momentum.

The $\psi^*(x + \frac{s}{2})$ and $\psi(x - \frac{s}{2})$ terms can be rewritten as given in the following equations:

$$\psi^*(x + \frac{s}{2}) = \langle \psi | x + \frac{s}{2} \rangle \quad (2.41)$$

$$\psi(x - \frac{s}{2}) = \langle x - \frac{s}{2} | \psi \rangle \quad (2.42)$$

Applying $1/2\pi$ to the third term of the Equation 2.40 (e^{ips}) and momentum eigenfunction in coordinate space with its complex conjugate, the third term becomes:

$$\frac{1}{2\pi} e^{ips} = \frac{1}{\sqrt{2\pi}} e^{ip(x+\frac{s}{2})} \frac{1}{\sqrt{2\pi}} e^{-ip(x-\frac{s}{2})} \quad (2.43)$$

It is possible to rewrite this equation as:

$$\frac{1}{\sqrt{2\pi}} e^{ip(x+\frac{s}{2})} \frac{1}{\sqrt{2\pi}} e^{-ip(x-\frac{s}{2})} = \langle x + \frac{s}{2} | p \rangle \langle p | x - \frac{s}{2} \rangle \quad (2.44)$$

By substitution of Equations 2.41, 2.42 and 2.44 into the Equation 2.40, the overall equation can be written as:

$$W(x, p) = \int_{-\infty}^{\infty} \langle \psi | x + \frac{s}{2} \rangle \langle x + \frac{s}{2} | p \rangle \langle p | x - \frac{s}{2} \rangle \langle x - \frac{s}{2} | \psi \rangle ds \quad (2.45)$$

The first term of the equation is the amplitude of a particle in the state ψ which has the position $(x - \frac{s}{2})$, the second term is the amplitude of a particle which has the position $(x - \frac{s}{2})$ with momentum p , the third term is the amplitude of a particle which has the momentum p with position $(x + \frac{s}{2})$ and the last term is the amplitude of a particle with position $(x + \frac{s}{2})$ in ψ state. Integration over s forms a superposition of all the possible quantum trajectories of ψ state, which is known to interfere both constructively and destructively, in the same time providing a quasi-probability distribution in the phase space (Figure 2.2) [68].

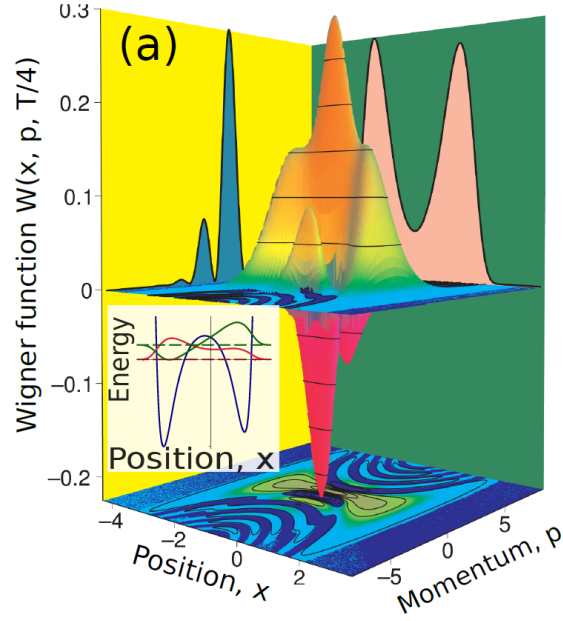


Figure 2.2. Wigner function graph $W(x,p)$, illustrating the momentum and the position probability distribution.

2.7. ϕ_S Index

ϕ_S index [69–71] is a descriptor of light-induced electronic charge density variation. It is a direct description which describes the charge transport during a light-absorption. ϕ_S index is obtained by analyzing the density matrices. Density matrix difference (Δ) is calculated by subtracting the ground state matrix (P_0) from the excited state density matrix P_X , as illustrated below:

$$\Delta = P_X - P_0 \Rightarrow \sum_{k=1}^K (\Delta S)_{kk} = 0 \quad (2.46)$$

in which the ΔS can be neglected. Because, the system does not gain or lose electrons. After a unitary similarity transformation is performed on Δ , the diagonal matrix δ can be written as:

$$\exists U | \delta = U^\dagger \Delta U; \quad (\delta)_{ij} = 0 \quad \forall i \neq j \quad (2.47)$$

The diagonal matrix is divided into two arrays according to their signs. Resultant diagonal matrices are transformed back in order to obtain the density matrices of the detachment (Γ) and the attachment (Λ). The detachment can be described as the deficiency in electron density that comes from the light absorption. Whereas, the attachment can be described as an increase in electron density at the excited state. They are expressed in the K atomic orbital space. By the fact that, no electron loss is observed during a vertical excitation, one can outline that:

$$\sum_{\mu=1}^K (\Gamma S)_{\mu\mu} = \sum_{\mu=1}^K (\Lambda S)_{\mu\mu} \quad (2.48)$$

Description of the detachment and attachment densities is also possible in 3D space. Spatial distribution of the electronic density removed from the ground state, namely detachment, and the reorganization in the excited state during the transition, namely attachment, are expressed by the equations below including the detached and the attached charge:

$$\theta = \int_R d\xi_1 \int_R d\xi_2 \int_R d\xi_3 \varrho_\tau(\xi_1 \xi_2 \xi_3) \equiv \int_{R^3} d^3 \xi \varrho_\tau(\xi) \quad (2.49)$$

$$\tau \equiv \Gamma, \Lambda \quad (2.50)$$

Thus, the ϕ_S index, without any dimension, can be expressed as the overlap between the attachment and the detachment densities:

$$\phi_S = \theta^{-1} \int_{R^3} d^3 \xi \sqrt{\varrho_\Gamma(\xi) \varrho_\Lambda(\xi)} \quad (2.51)$$

The ϕ_S index which is dependent on the charge-transfer character of the electronic transition, can have values in the range of 0 to 1. If the ϕ_S index is equal to 0, it means

that there is no overlap between the detachment and the attachment densities. On the other hand, if the descriptor is equal to 1 in an extreme case scenario, it means that there is no electronic density fluctuation between the ground state and the excited states (Figure 2.3).

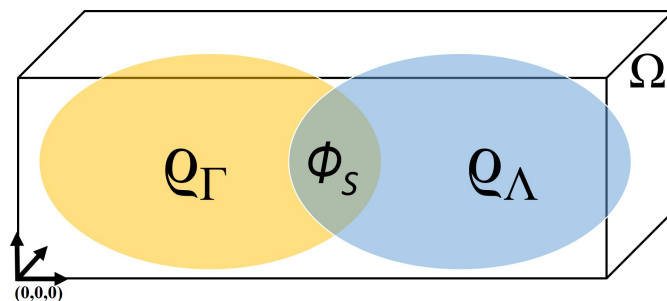


Figure 2.3. Graphical illustration of ϕ_S index as the overlap between detachment and attachment density matrices.

2.8. Fukui Functions

Local reactivity descriptors indicate preferred sites on a molecule where it would change its density when total numbers of electrons are modified by accepting or donating electrons. Fukui function is one of the local reactivity descriptors which can be utilized as a measure of reactivity. The Fukui functions allow prediction of the most electrophilic, nucleophilic and radicalic sites on a molecule by using DFT [72–75].

Fukui functions on a k^{th} atomic site, are defined for nucleophilic (f_k^+), electrophilic (f_k^-) and radical (f_k^0) attack as shown below:

$$f_k^+ = \rho_k(N + 1) - \rho_k(N) \quad (2.52)$$

$$f_k^- = \rho_k(N) - \rho_k(N - 1) \quad (2.53)$$

$$f_k^0 = \frac{\rho_k(N+1) - \rho_k(N-1)}{2} \quad (2.54)$$

where N is the number of electrons of a neutral molecule, ρ_k is the electron density at atomic position k of; neutral (N), anionic ($N+1$) and cationic ($N-1$) molecule.

We have calculated the electron density and spin density of atomic sites with Natural Population Analysis (NPA). Ground state optimized geometries of neutral molecules have been used for the calculations of the cation and the anion.

Parr and Yang showed that higher the value of a Fukui function higher the reactivity of that site in a molecule for the corresponding attack [76].

3. AIM OF THE STUDY

In this study, photophysical, kinetic and thermodynamic properties of novel *One-Component Type II* thioxanthone based photoinitiators have been investigated with the aim of understanding the initiation capabilities of the photoinitiators.

We have performed a series of calculations for assessing the level of theory in order to determine the best methodology which can be used for the computational calculations related to thioxanthone acetic acid derivatives.

After determination of the best methodology, vertical excitation properties of thioxanthone acetic acid derivatives have been calculated. UV-Vis spectra have been obtained from the vertical excitations with TD-DFT calculations and the corresponding frontier orbitals have been generated. In accordance with the TD-DFT calculations, dynamic and vibrational effects have been studied for the generation of more accurate UV-Vis spectra. The NTOs of the excitations have been calculated to understand the physical nature of the transitions.

Radical attack to monomer reactions of exocyclic and endocyclic radicals of thioxanthone acetic acid derivatives have been modelled in order to understand their initiating efficiency. In addition, phenyl acetic acid based radicals have been modelled to determine the differences and similarities between the *One-Component Type II* and *Type II* photoinitiation systems.

Spin densities and radical Fukui functions have been calculated for the initiating radicals to understand the reactivity of these species. Regression analyses for spin densities and radical Fukui functions have been carried out to establish a correlation with the activation energies.

4. RESULTS

4.1. Computational Procedure

All calculations have been carried out with Gaussian 09 (Ver. E.01.) software package [77]. DFT calculations at the B3LYP/6-31+G(d,p), M06-2X/6-31+G(d,p), ω B97X-D/6-31+G(d,p), B3LYP-D3/6-31+G(d,p) levels of theory have been carried out. 6-311++G(3df,3pd) basis set has been used for S atom in most of the calculations. Stationary points for all the minima have been characterized with positive frequencies, whereas transition structures have a unique negative frequency.

Electronic absorption spectra of thioxanthone acetic acid derivatives have been calculated with TD-DFT at B3LYP/6-31+G(d,p), M06-2X/6-31+G(d,p), ω B97X-D/6-31+G(d,p) levels in their most stable conformations with and without adding extra basis set (6-311++G(3df,3pd)) for S atom.

N, N'-Dimethylformamide (DMF) has been reported as the solvent in the polymerization reactions of thioxanthone acetic acid derivatives. For this reason, IEF-PCM has been used to mimic the same solvent environment. DMF with a dielectric constant of 37.219 [77] has been used as solvent implicitly in both DFT and in TD-DFT calculations.

Frontier orbitals have been generated from the TD-DFT calculations with Gaussian 09 software package. NTOs and ϕ_S values have been evaluated with Nancy_EX tool [69–71]. The NTOs have been visualized with the Avogadro software package [78].

In order to include dynamic and vibrational effects to our calculations, 20 snapshots of the optimized structures have been obtained from Q/P- uncorrelated quantum harmonic oscillator (Wigner) calculations by Newton-X Ver. 2 software package [79]. These snapshots have been used to generate more accurate UV-Vis spectra of thioxanthone acetic acid derivatives.

For the calculation of the radical Fukui functions, NPA have been carried out on the radical species and the electron density of the radical site on the molecule have been obtained.

4.2. Background

Synthesis of thioxanthone acetic acid derivatives is based on the incorporation of different acetic acid side groups to the thioxanthone core by the condensation reaction of thiosalicylic acid and an aromatic compound in the presence of concentrated sulfuric acid (Figure 1.9) [27]. Experimentally proposed radical formation mechanisms of thioxanthone acetic acid derivatives are given in Figure 4.1 and 4.2.

In both reactions, upon irradiation by a light source, thioxanthone acetic acid derivatives are known to reach a triplet state and make an intermolecular hydrogen abstraction spontaneously with decarboxylation and form two radicals; (i) exocyclic (blue) and (ii) endocyclic (red). Arsu *et al.* have proposed that the initiation is more favorable with the exocyclic radicals whereas the endocyclic radicals might lead to the formation of side products [35–37].

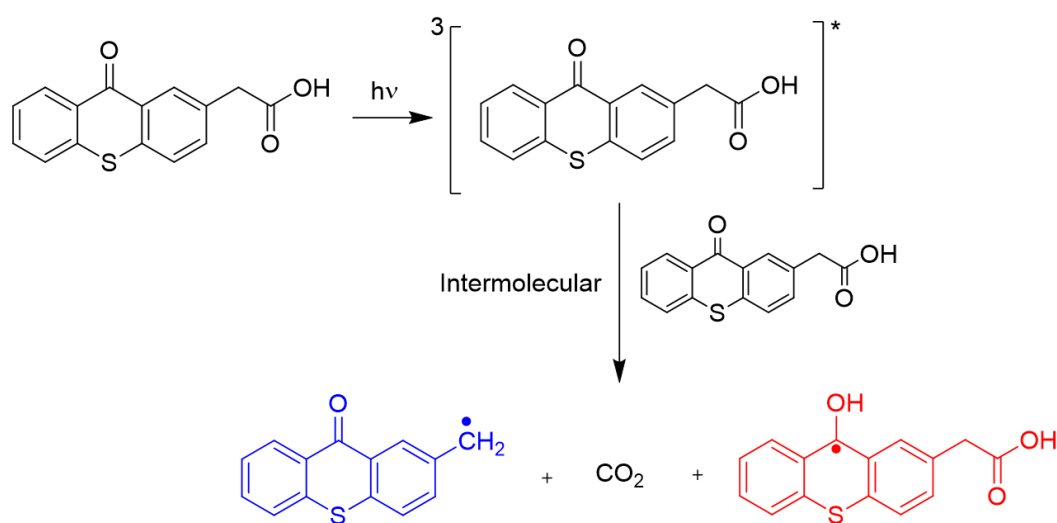


Figure 4.1. Experimentally proposed radical formation reaction of TX-AA.

Except for TX-AA, experimental studies suggest that there is a charge transfer between the thioxanthone molecules before the decarboxylation step [36,37]. Also, for some thioxanthone acetic acid derivatives, i.e. TX-O-AA and TX-S-AA, intramolecular interactions might be a possible route for the charge transfer [27].

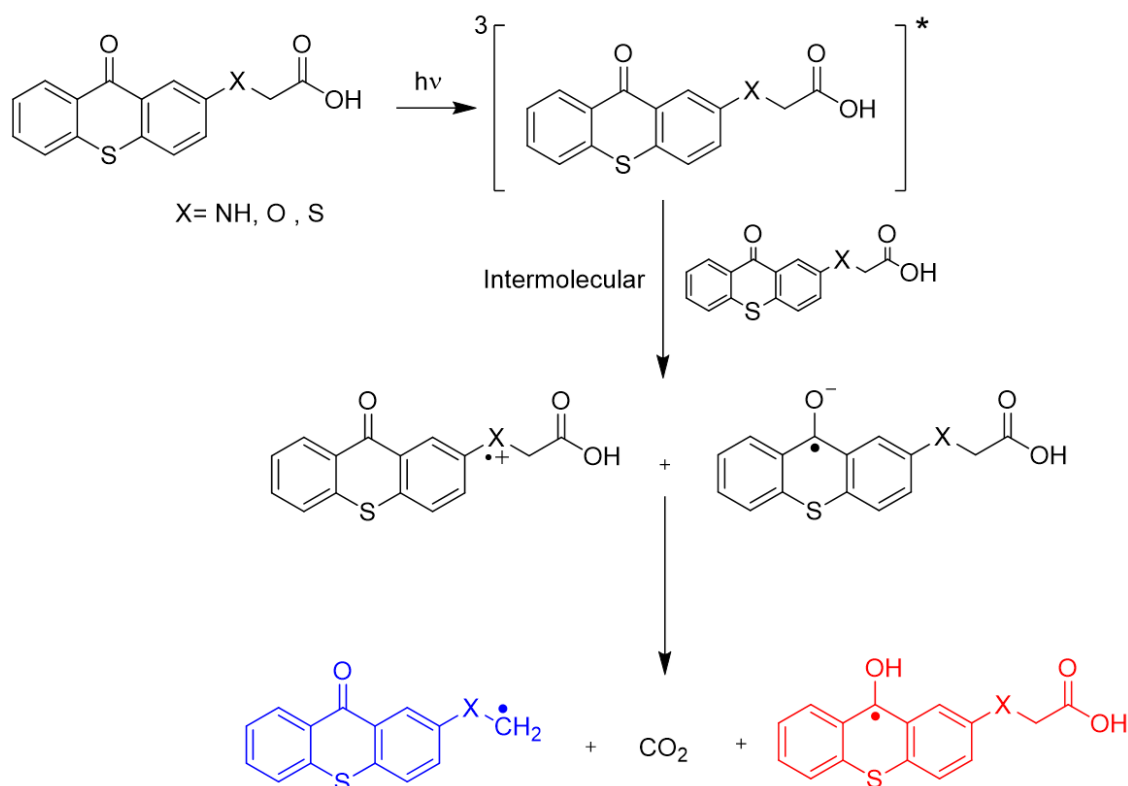


Figure 4.2. Experimentally proposed radical formation reaction of TX-NH-AA, TX-O-AA and TX-S-AA.

Thioxanthone, without any functional side group attached, is known to react as a *Type II* photoinitiator.

Phenyl acetic acid derivatives, especially *N*-phenylglycine, are well known co-initiators which are used in *Type II* photoinitiation systems [80–82]. Radical formation mechanisms of non-functionalized thioxanthone molecule with phenyl acetic acid based co-initiators are illustrated in Figure 4.3 and 4.4.

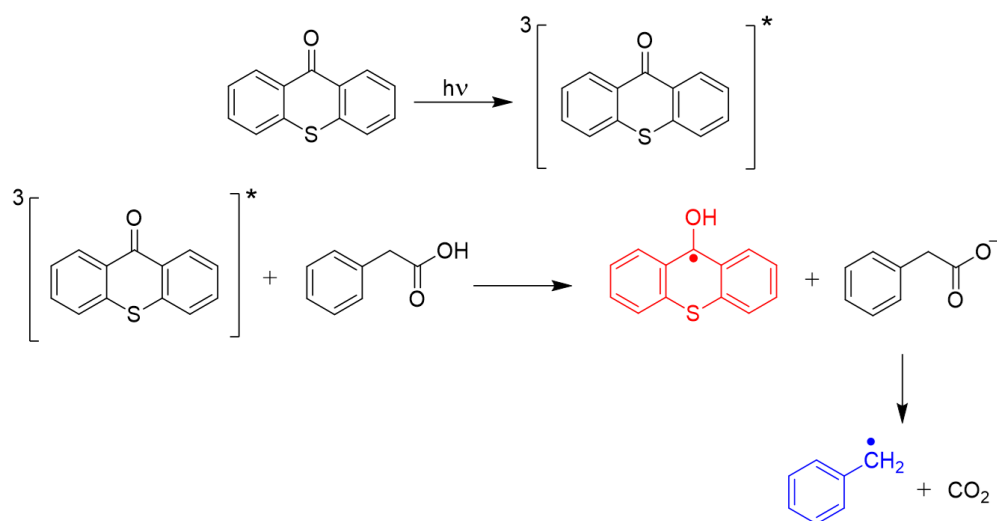


Figure 4.3. Radical formation reaction of PHC.

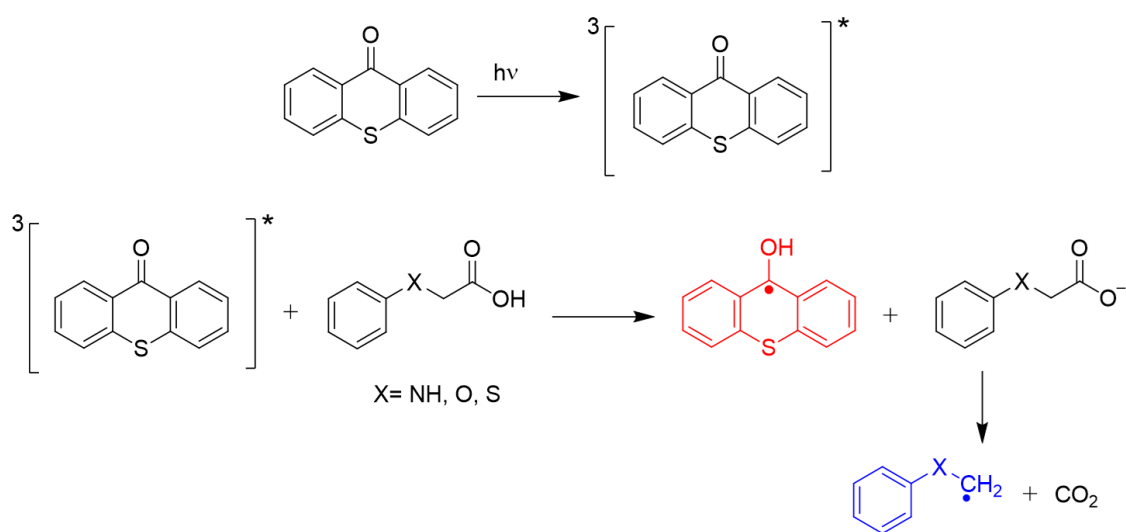


Figure 4.4. Radical formation reaction of PHN, PHO and PHS.

In contrast to *One-Component Type II* photoinitiation reactions of thioxanthone acetic acid derivatives, conventional *Type II* photoinitiation reactions of phenyl acetic acid derivatives with thioxanthone, lead to the formation of endocyclic radical on the thioxanthone core (red). Endocyclic radical is formed after the thioxanthone reaches triplet state and makes an intermolecular hydrogen abstraction from the co-initiator molecule. Hydrogen abstraction is followed by decarboxylation and consequently the exocyclic radical on the co-initiator (blue) forms (Figure 4.3 and 4.4).

Radical attack to monomer reaction rate is an important indicator for the efficiency of the photopolymerization reactions, since it is the first step in the photopolymerization after the formation of radicals [83–85].

In this study, we have modelled the radical attack to the monomer both for exocyclic and endocyclic radicals of thioxanthone acetic acid derivatives in order to understand the competition between these radicals which are assumed to co-exist in the *One-Component Type II* photoinitiation reactions (Figure 4.5) [35–37].

Phenyl acetic acid based co-initiators and *One-Component Type II* thioxanthone acetic acid based photoinitiators have the same acetic acid based side groups on their structures. For this reason, in order to understand the similarities and the differences between the initiation capabilities of *One-Component Type II* and *Type II* photoinitiators, exocyclic radical attack of phenyl acetic acid derivatives (co-initiators) and the endocyclic radical attack of non-functionalized thioxanthone (photoinitiator) have been modelled concurrently (Figure 4.5).

Methyl methacrylate (MMA) monomer usage has been reported in the polymerization studies of thioxanthone acetic acid derivatives [35–37]. In order to design similar reaction conditions, MMA has been selected as the monomer through all modelled initiation reactions of thioxanthone acetic acid based and phenyl acetic acid based radicals.

Simulating similar reaction conditions by the usage of the same monomer and the same solvent have led to more accurate and meaningful comparisons related to the initiation capabilities of the formed radicals.

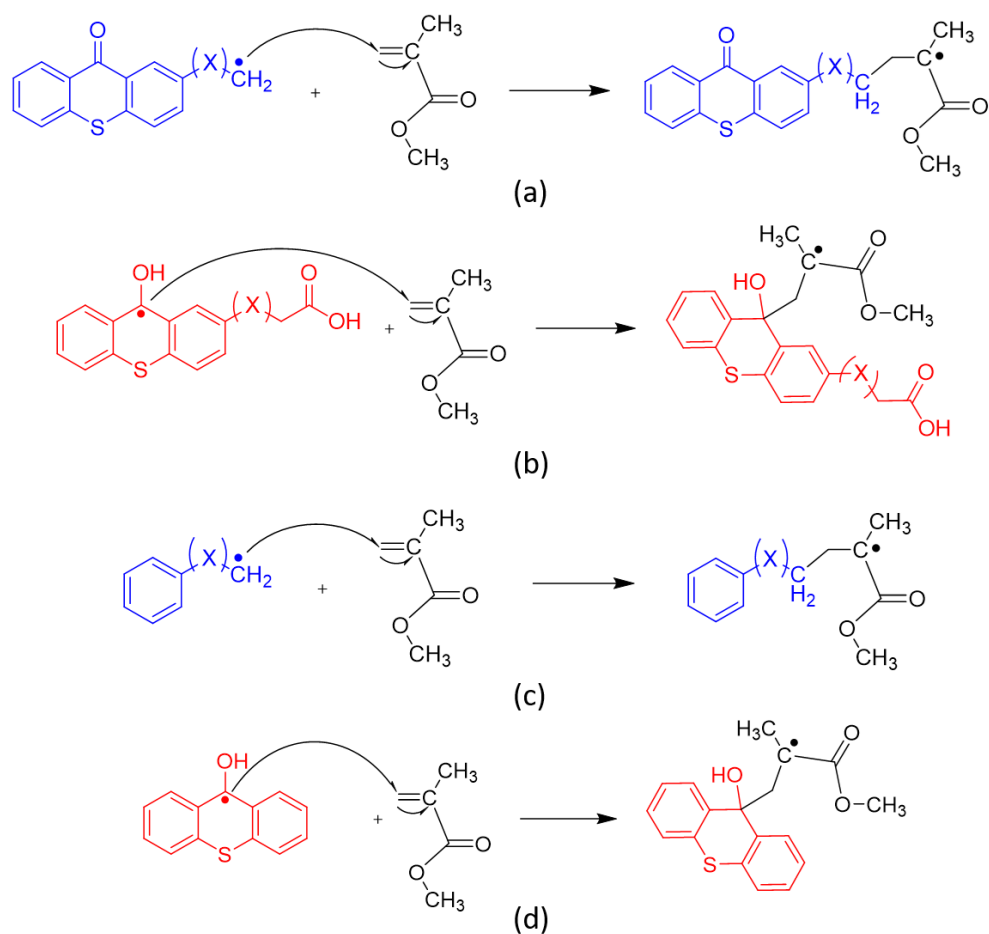


Figure 4.5. Initiation reactions modeled in this study (X:NH, O, S).

In Figure 4.5 (a) and (b) stands for exocyclic and endocyclic radical attack of thioxanthone acetic acid derivatives respectively, (c) for exocyclic radical attack of phenyl acetic acid derivatives and (d) for endocyclic radical attack of thioxanthone to MMA.

4.3. Assessing the Level of Theory

4.3.1. Energetics

In computational chemistry, assessing the level of theory is crucial for the determination of the best methodology that produces the experimental results accurately. This is true especially for novel synthetic molecules. As mentioned in detail in the Methodology chapter, there are a wide variety of functionals and basis sets available for the computation.

We have used different functionals (B3LYP, M06-2X, ω B97X-D and B3LYP-D3) with the basis sets 6-31+G(d,p) and 6-311++G(3df,3pd) for S atom, to model the initiation reactions and at the same time to generate the UV-Vis spectra by vertical excitations from the ground state.

Change in the free energy of activation with different functionals for the exocyclic radicals of thioxanthone, are given in Figure 4.6. ΔG^\ddagger have been calculated by the subtraction of the energy of the transition state complex from the sum of the energies of the minimum energy conformations of the corresponding reactants, exocyclic radical and the MMA. Adding extra basis set for S atom have made almost no change in the free energy of activation value within the same functional for all tested methodologies. A general trend between the activation energies of molecules has been observed within the framework of different functionals used whereas calculations with ω B97X-D and B3LYP-D3 do not show the same pattern.

Determination of the more accurate methodology was accomplished after the generation of UV-Vis spectra.

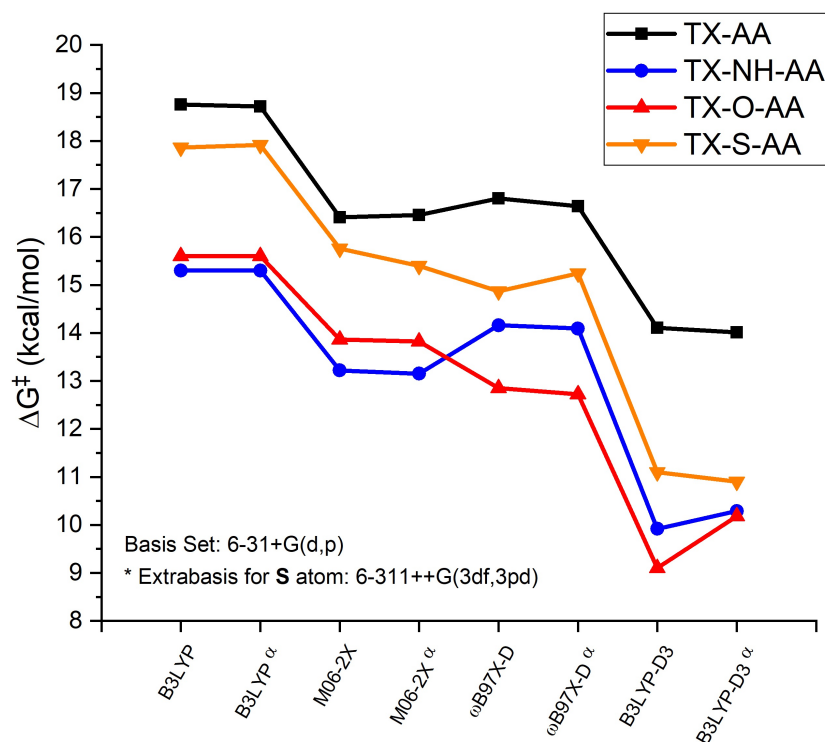


Figure 4.6. Free energy of activation with different functionals in the exocyclic radical attack to MMA reactions of thioxanthone acetic acid derivatives.

The pre-reactive complexes (PRCs) are higher in energy than the total energy of the corresponding reactants. Thus, the activation energies are calculated as the difference between the free energy of the transition state structure and the sum of free energies of the reactants.

Relative energies of each molecule structure in exocyclic radical attack to MMA reactions of thioxanthone acetic acid derivatives are given in detail in Table 4.1. In general, calculations carried out with M06-2X and ω B97X-D have resulted in lower energies of intermediates than the calculations carried out with B3LYP and B3LYP-D3. Note that all reactions possess exergonic behaviour with each functional used.

Table 4.1. Relative Gibbs energies (kcal/mol) for the transition states, intermediates and PRCs in the reactions of exocyclic radical attack to MMA.

Molecule	Methodology ^{a,b}	TS	Int.	PRC
TX-AA _{exo}	B3LYP	18.72	-2.28	4.92
	M06-2X	16.46	-9.60	5.74
	ω B97X-D	16.64	-10.21	4.19
	B3LYP-D3	14.01	-6.64	3.06
TX-NH-AA _{exo}	B3LYP	15.30	-4.14	5.29
	M06-2X	13.15	-12.26	5.74
	ω B97X-D	14.09	-12.66	6.18
	B3LYP-D3	10.29	-8.43	3.50
TX-O-AA _{exo}	B3LYP	15.60	-11.41	7.29
	M06-2X	13.82	-19.30	5.44
	ω B97X-D	12.72	-19.81	4.97
	B3LYP-D3	10.18	-17.42	2.73
TX-S-AA _{exo}	B3LYP	17.92	-6.40	5.98
	M06-2X	15.40	-15.55	5.15
	ω B97X-D	15.24	-16.08	3.43
	B3LYP-D3	10.90	-13.05	4.30
^a 6-31 + G(d, p)				
^b Extra basis set for S atom: 6-311++G(3df,3pd)				

4.3.2. Vertical Excitations

We have performed a series of TD-DFT calculations with the optimized ground state structures and UV-Vis spectra have been generated.

M06-2X/6-31+G(d,p) and ω B97X-D/6-31 + G(d, p) methodologies have failed to represent the experimental data. Calculated absorption maximum values were located at significantly lower wavelengths for all thioxanthone acetic acid derivatives.

B3LYP/6-31+G(d,p) methodology has been the most successful to generate the UV-Vis spectrum among the other methodologies used. Including extra basis set for the S atom (6-311++G(3df,3pd)) have generated even more accurate results.

Previously, Wang *et al.* [42], Li *et al.* [43], Sun *et al.* [44] and Beni *et al.* [45,46] have also reported the accuracy of B3LYP in their studies. Wang *et al.*, Li *et al.* and Sun *et al.* have used B3LYP for the optimization and vertical excitation studies of thioxanthone based molecules for the design of TADF emitters. Beni *et al.* have carried out series of DFT calculations on thioxanthone and hydroxythioxanthenes to define the molecular, geometric and photophysical properties of the molecules. In the same manner, our results also suggest that B3LYP functional is an adequate functional to be used for modelling thioxanthone based molecules.

Singlet excitation properties of TX-AA, TX-NH-AA, TX-O-AA and TX-S-AA are given in Table 4.2 to 4.5, in which α denotes addition of extra basis set (6-311++G(3df,3pd)) for S atom, excitation energies are in eV, wavelength in nm, (f) is oscillator strength, (H) stands for HOMO and (L) stands for LUMO, (%) denotes contribution % and (c) is the coefficient.

Table 4.2. Singlet Excitation Properties of TX-AA with different methodologies.

Methodology	eV	nm	f	Nature	%	c
M06-2X	3.8435	322.58	0.0462	H(-4) \rightarrow L	58.72	0.54187
				H \rightarrow L	31.29	0.39551
ω B97X-D	3.8647	320.81	0.1460	H \rightarrow L	94.61	0.68778
B3LYP	3.3485	370.27	0.0960	H \rightarrow L	96.61	0.69501
B3LYP $^{\alpha}$	3.3224	373.18	0.0928	H \rightarrow L	96.57	0.69486

Table 4.3. Singlet Excitation Properties of TX-NH-AA with different methodologies.

Methodology	eV	nm	f	Nature	%	c
M06-2X	3.4390	360.52	0.1279	H \rightarrow L	96.03	0.69293
ω B97X-D	3.4428	360.13	0.1303	H \rightarrow L	93.77	0.68474
B3LYP	2.8535	434.49	0.0799	H \rightarrow L	98.25	0.70089
B3LYP $^{\alpha}$	2.8476	435.39	0.0788	H \rightarrow L	98.19	0.70068

Table 4.4. Singlet Excitation Properties of TX-O-AA with different methodologies.

Methodology	eV	nm	f	Nature	%	c
M06-2X	3.7051	334.63	0.1510	H \rightarrow L	96.41	0.69431
ω B97X-D	3.7093	334.25	0.1549	H \rightarrow L	95.07	0.68947
B3LYP	3.2028	387.11	0.1004	H \rightarrow L	97.16	0.69698
B3LYP $^{\alpha}$	3.1809	389.78	0.0970	H \rightarrow L	97.10	0.69679

Table 4.5. Singlet Excitation Properties of TX-S-AA with different methodologies.

Methodology	eV	nm	f	Nature	%	c
M06-2X	3.8302	323.71	0.0020	H(-5) → L	80.93	0.63614
				H(-5) → L(+22)	3.51	-0.13239
ω B97X-D	3.8751	319.95	0.1294	H → L	93.59	0.68406
B3LYP	3.3388	371.35	0.0808	H → L	96.40	0.69425
B3LYP $^{\alpha}$	3.3062	375.01	0.0757	H → L	96.36	0.69412

4.4. Absorption Properties and Frontier Orbitals

Ground state optimized geometries and vertical excitation properties with reported experimental values [35–37] of thioxanthone acetic acid derivatives, calculated with B3LYP/6-31+G(d,p) for S: 6-311++G(3df,3pd) in DMF, are given in Figure 4.7 and Table 4.6, respectively.

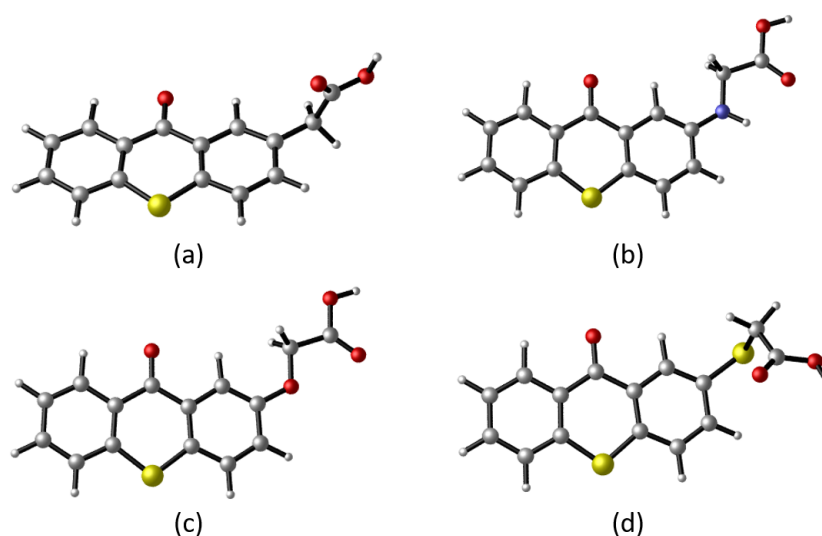


Figure 4.7. Ground state geometries of thioxanthone acetic acid derivatives (a) TX-AA, (b) TX-NH-AA, (c) TX-O-AA and (d) TX-S-AA.

In Table 4.6 excitation energies in eV, wavelength in nm, oscillator strength (f), contribution % , coefficient (c) and experimental wavelength in nm, are reported.

Main transitions for all thioxanthone acetic acid derivatives are from HOMO to LUMO with the contribution % values in the range of 96.36 to 98.19. A correlation between the experimental and calculated UV-Vis absorption values have been observed.

Table 4.6. Singlet excitation properties of thioxanthone acetic acid derivatives (B3LYP/6-31+G(d,p) for S: 6-311++G(3df,3pd) in DMF).

Molecule	eV	Wav.	f	Nature	%	c	Exp. Wav.
TX-AA	3.3224	373.18	0.0928	H → L	96.57	0.69486	384
TX-NH-AA	2.8476	435.39	0.0788	H → L	98.19	0.70068	392-430
TX-O-AA	3.1809	389.78	0.0970	H → L	97.10	0.69679	380-400
TX-S-AA	3.3062	375.01	0.0757	H → L	96.36	0.69412	380-400

Even though the quantitatively minimum energy conformer in TD-DFT calculations represents the photophysical properties of the system well, the simulated absorption characteristics match with the experimental data better when the vibrational effects are included on the geometry by Wigner distribution method. It is known that, single-conformation dynamic approach applied by the Wigner distribution is capable of reproducing the optical properties of organic chromophores of different structures almost quantitatively [86–89].

On that account, in order to produce more accurate UV-Vis absorption characteristics, Q/P-uncorrelated quantum harmonic oscillator (Wigner) method have been used to generate UV-Vis spectra of the molecules. By applying this method to our calculations, more precise spectra which match the experimental data have been obtained (Figure 4.8 to 4.11).

In conjunction with assessing the level of theory, generation of more precise UV-Vis spectra with B3LYP/6-31+G(d,p) for S: 6-311++G(3df,3pd) in DMF through Wigner calculations have led us to select this methodology for the further calculations.

According to the reported experimental UV-Vis measurements; TX-NH-AA has showed a tailing effect in UV-Vis spectrum between the range of 392 to 430 nm [27,36]. Even though this tailing effect has been observed in experimental studies, it has not been observed in computational calculations. However, a corresponding peak has been observed in the same region of the tailing effect (Figure 4.8).

TX-NH-AA is known as panchromatic photoinitiator, the shift to longer wavelengths is due to the hydrogen bonding ability of glycine functionality on the molecule [27,36]. Our goal was to determine the best methodology to reproduce experimental results by comparing the calculated and experimental UV-Vis spectra. For this reason, hydrogen bonding capabilities with the medium have not been considered in this study.

TX-AA, TX-O-AA and TX-S-AA molecules have shown a large absorption maximum peak in the range of 380-400 nm [36–38]. Accurate UV-Vis spectra for these molecules have been obtained in our calculations (Figure 4.9 to 4.11).

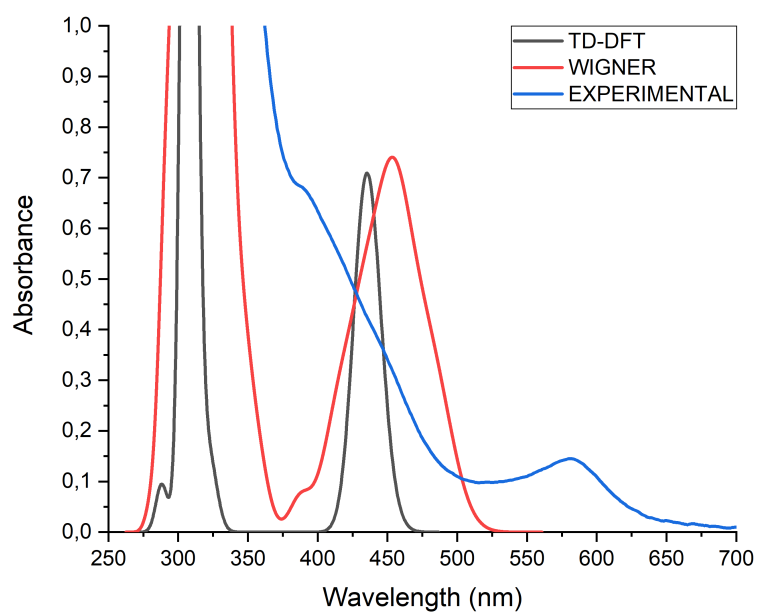


Figure 4.8. Calculated and experimental UV-Vis absorption spectra of TX-NH-AA.

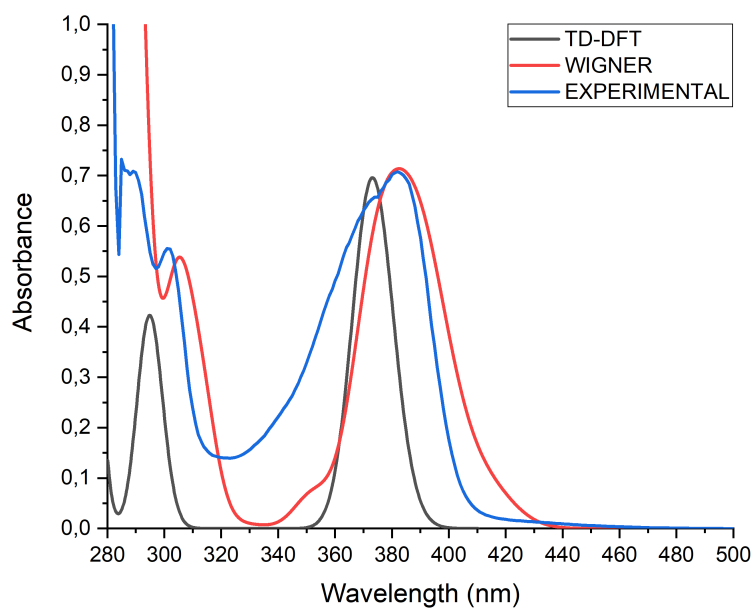


Figure 4.9. Calculated and experimental UV-Vis absorption spectra of TX-AA.

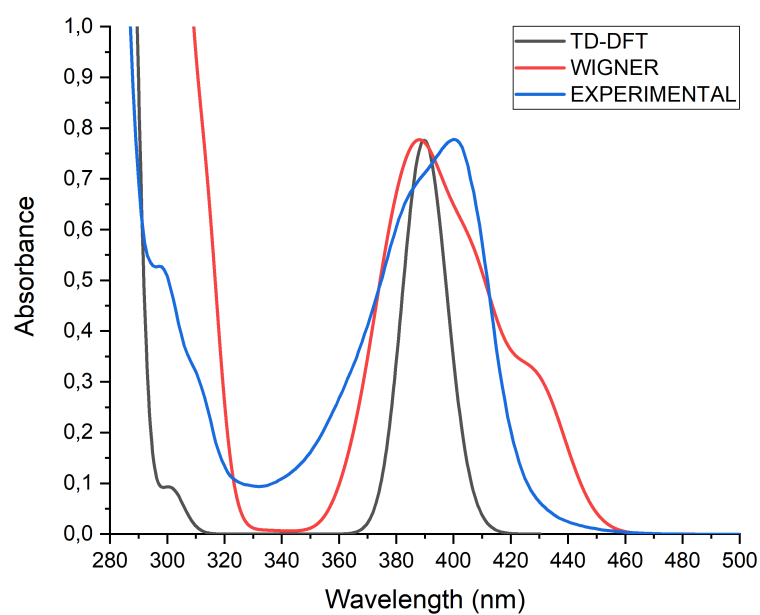


Figure 4.10. Calculated and experimental UV-Vis absorption spectra of TX-O-AA.

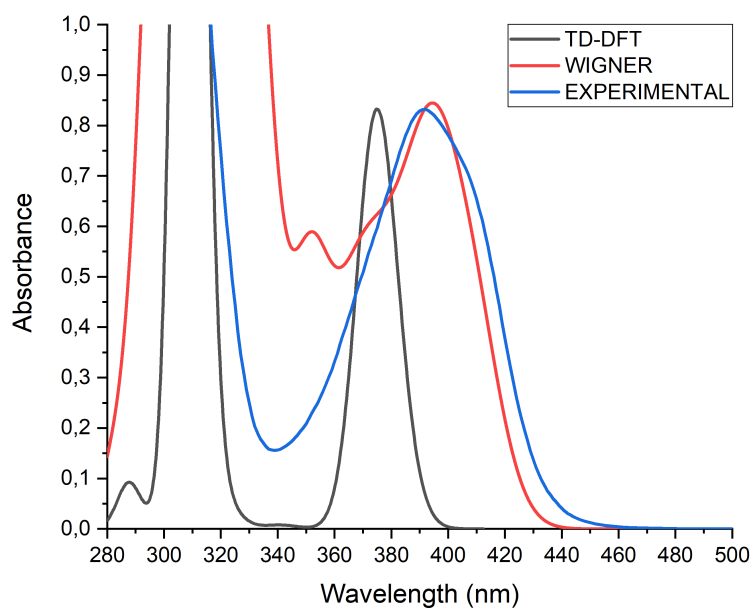
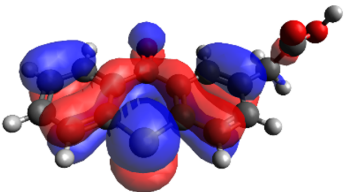
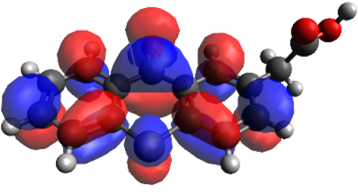
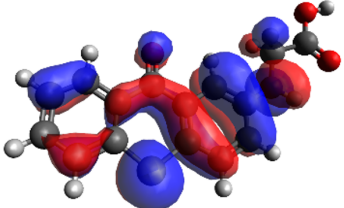
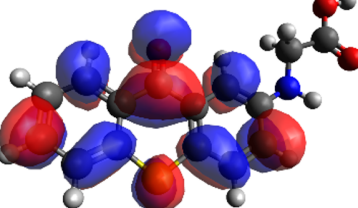
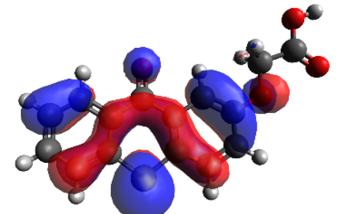
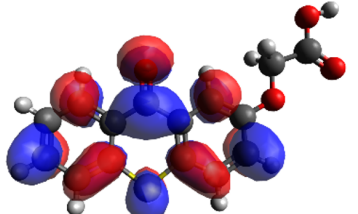
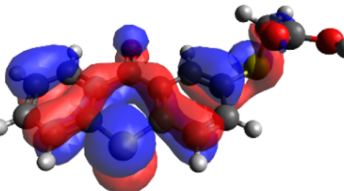
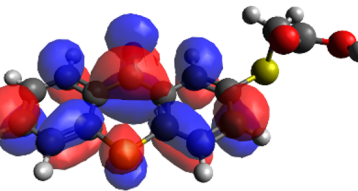


Figure 4.11. Calculated and experimental UV-Vis absorption spectra of TX-S-AA.

Dominant transition of thioxanthone acetic acid derivatives is $S_0 \rightarrow S_1$. Frontier orbitals (HOMO and LUMO) related to these transitions of thioxanthone acetic acid derivatives, are given in Table 4.7.

Table 4.7. Frontier orbitals of thioxanthone acetic acid derivatives
(B3LYP/6-31+G(d,p) for S: 6-311++G(3df,3pd) in DMF).

Molecule	HOMO	LUMO
TX-AA		
TX-NH-AA		
TX-O-AA		
TX-S-AA		

4.5. Natural Transition Orbitals

A possible route to improve the understanding of the physical nature of electronic transitions is the analysis of the corresponding NTOs. This way, one can express the excited state in terms of transitions from occupied and virtual NTOs.

Occupied and virtual NTOs of thioxanthone acetic acid derivatives with calculated parameters of transitions, are given in Table 4.8 to 4.11. The first vertical transition ($S_0 \rightarrow S_1$) of all thioxanthone acetic acid derivatives have $\pi - \pi^*$ nature which can be also followed by the generated UV-Vis spectra.

Addition of NH, O, and S atoms between the thioxanthone core influences the occupied NTOs (oNTOs) whereas not the virtual NTOs (vNTOs) (Table 4.8 to 4.11).

Calculated ϕ_S -Löwdin values are in the range of 0.695 - 0.725, lowest being the TX-NH-AA and highest being the TX-S-AA. ϕ_S -Mulliken values are in the range of 0.726 - 0.733 and again lowest being the TX-NH-AA and highest being the TX-S-AA.

ϕ_S values of the $S_0 \rightarrow S_1$ transitions for all thioxanthone acetic acid derivative is close to 1 and this verifies the local excitation character of the transitions. For all thioxanthone acetic acid derivatives only $S_0 \rightarrow S_2$ transitions have ϕ_S values close to 0, however their oscillator strength is 0.

Table 4.8. Occupied and virtual NTOs of TX-AA with calculated parameters of transitions (B3LYP/6-31+G(d,p) for S: 6-311++G(3df,3pd) in DMF).

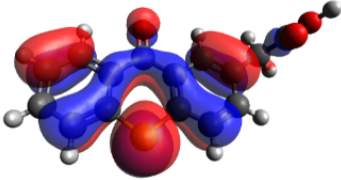
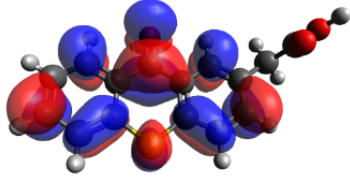
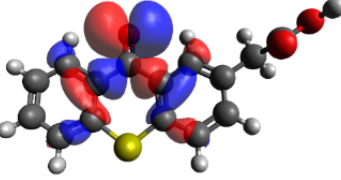
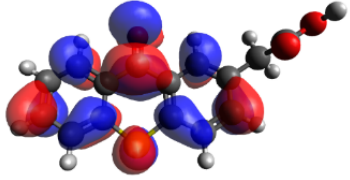
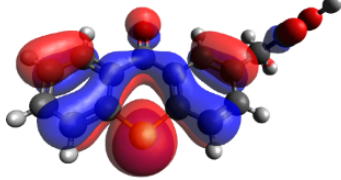
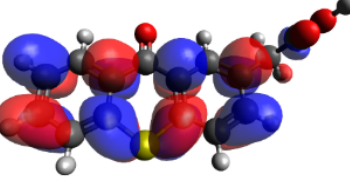
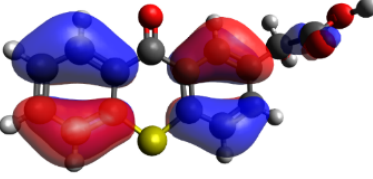
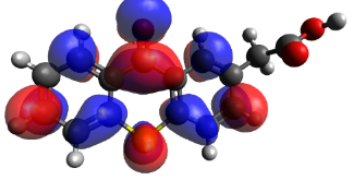
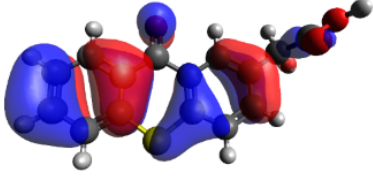
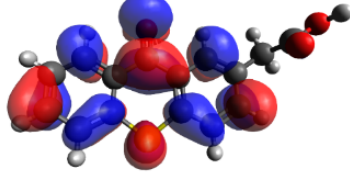
Parameters	oNTO	vNTO
$S_0 \rightarrow S_1$ 3.3224 eV $f = 0.0928$ ϕ_S -Löwdin = 0.701 ϕ_S -Mulliken = 0.723		
$S_0 \rightarrow S_2$ 3.6656 eV $f = 0.0000$ ϕ_S -Löwdin = 0.378 ϕ_S -Mulliken = 0.396		
$S_0 \rightarrow S_3$ 4.2046 eV $f = 0.0564$ ϕ_S -Löwdin = 0.849 ϕ_S -Mulliken = 0.864		
$S_0 \rightarrow S_4$ 4.5557 eV $f = 0.1364$ ϕ_S -Löwdin = 0.749 ϕ_S -Mulliken = 0.755		
$S_0 \rightarrow S_5$ 4.6607 eV $f = 0.7542$ ϕ_S -Löwdin = 0.834 ϕ_S -Mulliken = 0.840		

Table 4.9. Occupied and virtual NTOs of TX-NH-AA with calculated parameters of transitions (B3LYP/6-31+G(d,p) for S: 6-311++G(3df,3pd) in DMF).

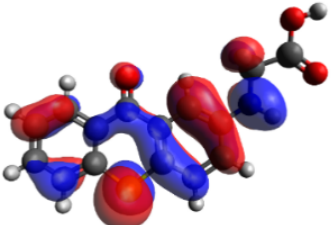
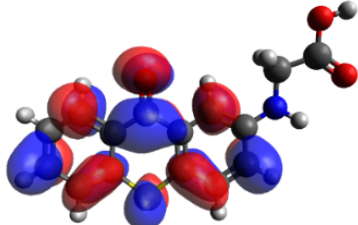

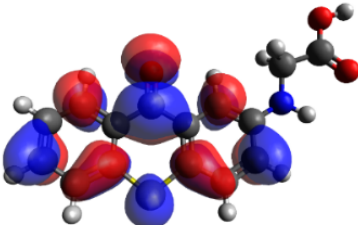
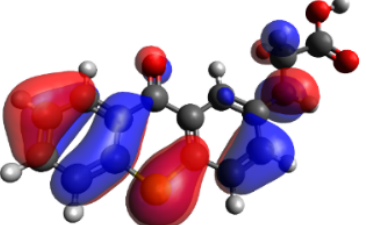
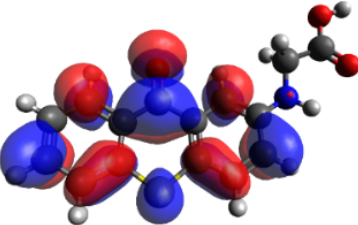
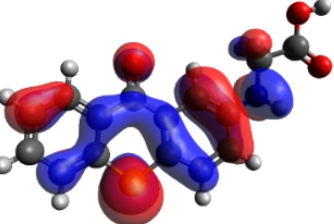
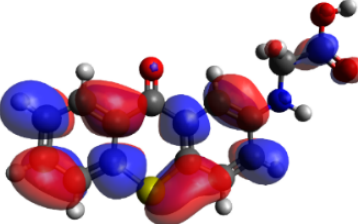
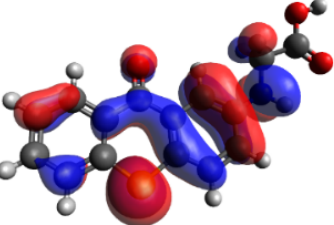
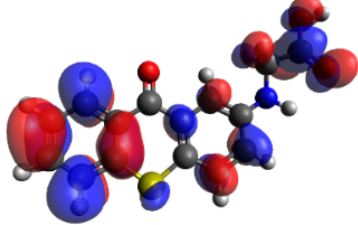
Parameters	oNTO	vNTO
$S_0 \rightarrow S_1$ 2.8476 eV $f = 0.0788$ ϕ_S -Löwdin = 0.695 ϕ_S -Mulliken = 0.726		
$S_0 \rightarrow S_2$ 3.6719 eV $f = 0.0000$ ϕ_S -Löwdin = 0.301 ϕ_S -Mulliken = 0.320		
$S_0 \rightarrow S_3$ 3.8441 eV $f = 0.0156$ ϕ_S -Löwdin = 0.829 ϕ_S -Mulliken = 0.842		
$S_0 \rightarrow S_4$ 4.0278 eV $f = 0.3065$ ϕ_S -Löwdin = 0.797 ϕ_S -Mulliken = 0.813		
$S_0 \rightarrow S_5$ 4.3013 eV $f = 0.0105$ ϕ_S -Löwdin = 0.566 ϕ_S -Mulliken = 0.599		

Table 4.10. Occupied and virtual NTOs of TX-O-AA with calculated parameters of transitions (B3LYP/6-31+G(d,p) for S: 6-311++G(3df,3pd) in DMF).

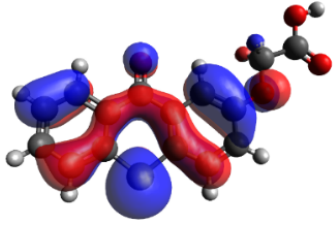
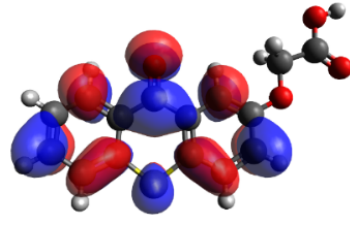
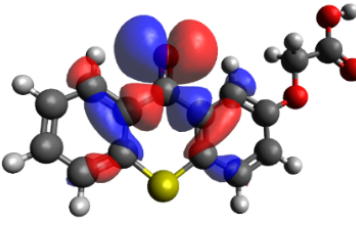
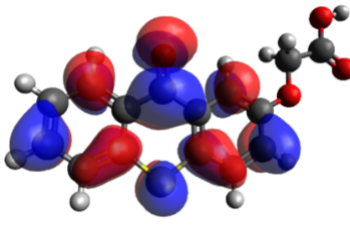
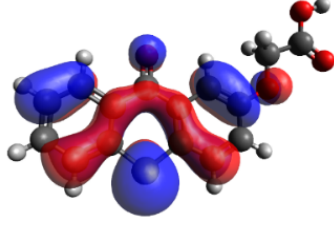
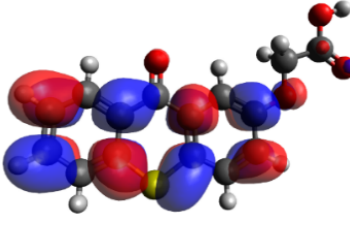
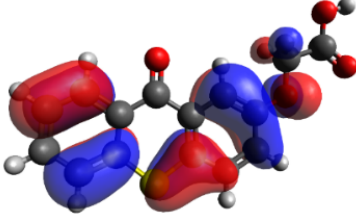
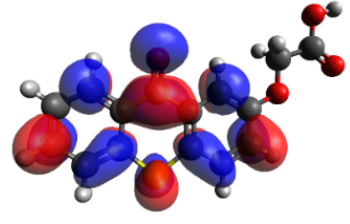
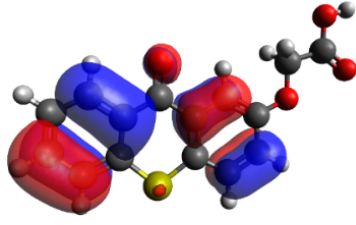
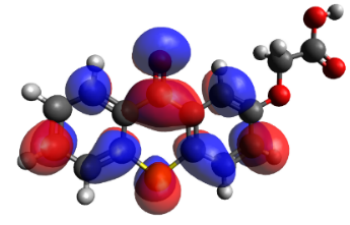
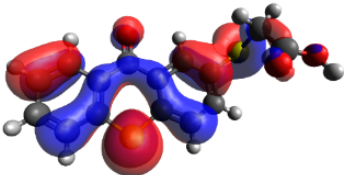
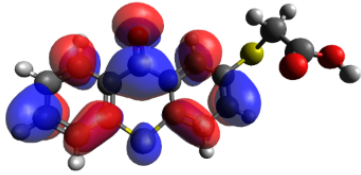
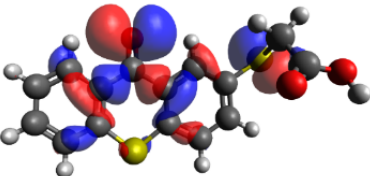
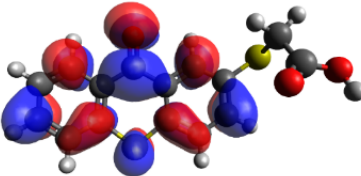
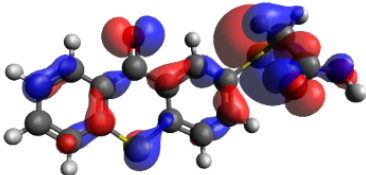
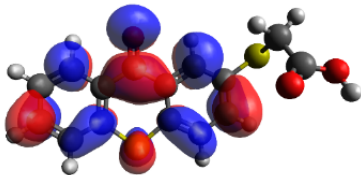
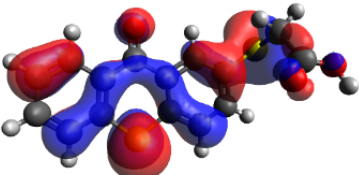
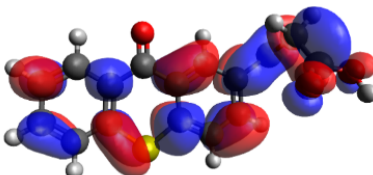
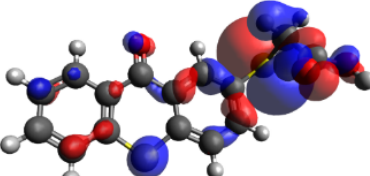
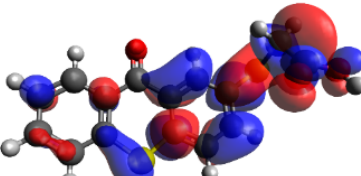
Parameters	oNTO	vNTO
$S_0 \rightarrow S_1$ 3.1809 eV $f = 0.0970$ ϕ_S -Löwdin = 0.712 ϕ_S -Mulliken = 0.732		
$S_0 \rightarrow S_2$ 3.6748 eV $f = 0.0000$ ϕ_S -Löwdin = 0.262 ϕ_S -Mulliken = 0.280		
$S_0 \rightarrow S_3$ 4.1180 eV $f = 0.0113$ ϕ_S -Löwdin = 0.862 ϕ_S -Mulliken = 0.871		
$S_0 \rightarrow S_4$ 4.3510 eV $f = 0.2219$ ϕ_S -Löwdin = 0.775 ϕ_S -Mulliken = 0.783		
$S_0 \rightarrow S_5$ 4.5567 eV $f = 0.4151$ ϕ_S -Löwdin = 0.793 ϕ_S -Mulliken = 0.801		

Table 4.11. Occupied and virtual NTOs of TX-S-AA with calculated parameters of transitions (B3LYP/6-31+G(d,p) for S: 6-311++G(3df,3pd) in DMF).

Parameters	oNTO	vNTO
$S_0 \rightarrow S_1$ 3.3062 eV $f = 0.0757$ ϕ_S -Löwdin = 0.725 ϕ_S -Mulliken = 0.733		
$S_0 \rightarrow S_2$ 3.6373 eV $f = 0.0007$ ϕ_S -Löwdin = 0.372 ϕ_S -Mulliken = 0.405		
$S_0 \rightarrow S_3$ 3.4287 eV $f = 0.0034$ ϕ_S -Löwdin = 0.688 ϕ_S -Mulliken = 0.739		
$S_0 \rightarrow S_4$ 4.0141 eV $f = 0.2635$ ϕ_S -Löwdin = 0.830 ϕ_S -Mulliken = 0.859		
$S_0 \rightarrow S_5$ 4.3085 eV $f = 0.0084$ ϕ_S -Löwdin = 0.677 ϕ_S -Mulliken = 0.714		

As previously mentioned, transitions are mainly located on the thioxanthone core. However, contribution of NH group, O and S atom to the transitions with minor effects can be observed in the generated orbitals.

Even though these groups have minor effects on the transitions (on oNTOs), contribution of the acetic acid group is not observable. This can be verified by the inspection of the $S_0 \rightarrow S_1$ NTOs of TX-AA, where no additional group is present between the thioxanthone core and the acetic acid side group.

4.6. Kinetic and Thermodynamic Properties of Reactions

After the successful generation of UV-Vis spectra of the thioxanthone acetic acid derivatives and the determination of the functional and basis set to be used in further calculations, we have modelled the radical formation and the initiation reactions of thioxanthone acetic acid based radicals (TX-AA_{exo}, TX-NH-AA_{exo}, TX-O-AA_{exo}, TX-S-AA_{exo}) with endocyclic radicals (TX-AA_{endo}, TX-NH-AA_{endo}, TX-O-AA_{endo}, TX-S-AA_{endo}). Additionally, initiation reactions of phenyl acetic acid based radicals (co-initiators) (PHC_{exo}, PHN_{exo}, PHO_{exo} and PHS_{exo}) and the thioxanthone (*Type II* photoinitiator) (TX_{endo}) have been modelled. The following sections are dedicated to these reactions.

4.6.1. Radical Formation Reactions

If you refer to Figure 4.1 and 4.2, an intermolecular H-abstraction have been proposed for thioxanthone acetic acid derivatives and phenyl acetic acid derivatives followed by decarboxylation. In Figure 4.12, overall reactions of radical formation are given.

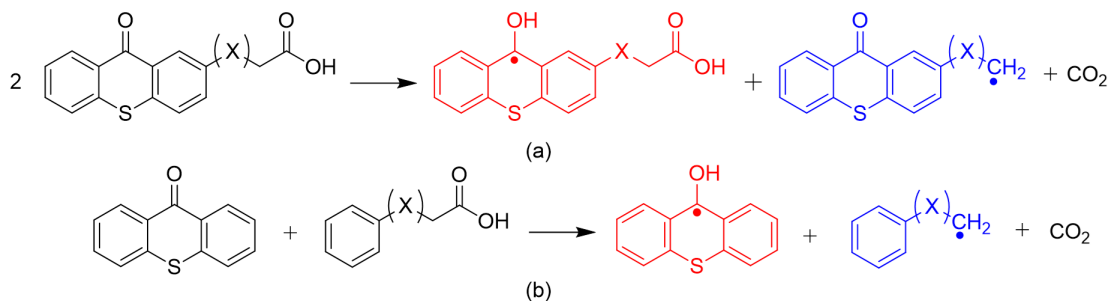


Figure 4.12. Overall radical formation reactions of (a) thioxanthone acetic acid derivatives and (b) phenyl acetic acid derivatives (X:NH, O, S).

We have calculated the overall reaction Gibbs free energy of these reactions to be able to compare thermodynamic properties of the radical formation reactions. Table 4.12 summarizes the overall reaction Gibbs free energies of radical formation, calculated with B3LYP/6-31+G(d,p) for S: 6-311++G(3df,3pd) in DMF.

Table 4.12. Overall reaction Gibbs free energies (ΔG_{rxn}^o , kcal/mol) of radical formation.

Molecule	ΔG_{rxn}^o	Molecule	ΔG_{rxn}^o
TX-AA	32.52	PHC	33.07
TX-NH-AA	34.73	PHN	34.15
TX-O-AA	40.16	PHO	40.09
TX-S-AA	34.57	PHS	35.71

Radical formation reactions consist of multiple steps; excitation to triplet state, intermolecular hydrogen abstraction followed by decarboxylation and the subsequently radical formation. Overall reactions for all species have possessed a strong endergonic character (Table 4.12). It is widely known that, radical formation by irradiation is an endergonic process where the required energy is provided by a light source. Our findings correlate with this common knowledge.

4.6.2. Initiation Reactions

Radical formation reactions are endergonic reactions where the structural design and complexity of the side groups can affect the endergonic character of the overall reaction. However, the driving energy can be easily provided by the light sources. If the energy of the light source is not efficient, variety of the parameters can be utilized to initiate the radical formation reactions such as; changing the wavelength, changing the distance between the light source and the reaction media, total time of irradiation and more. In any case, radical formation of the photoinitiator can be accomplished. On the other hand, formed radicals take over the overall performance of the photopolymerization, by their initiation capabilities, once they are formed.

We have modelled the initiation reactions and calculated spin densities of all possible radicals that can co-exist in the reaction media. Exocyclic and endocyclic radicals of thioxanthone acetic acid derivatives, exocyclic radicals of the phenyl acetic acid based co-initiators and the endocyclic radical of non-functionalized thioxanthone (*Type II* photoinitiator) have been modelled step by step. Initiation capabilities of these radicals have been compared within the same photoinitiator types also between the *One-Component Type II* system and *Type II* system by the comparison of the calculated kinetic and thermodynamic parameters.

Reactions rate constants have been calculated by the Eyring's Equation (Equation 4.1) [90].

$$k = \frac{k_B \cdot T}{h} \cdot \frac{RT}{P_0} \cdot e^{-\Delta G^\ddagger/RT} \quad (4.1)$$

where k is reaction rate constant ($\text{L}\cdot\text{mol}^{-1}\cdot\text{s}^{-1}$), k_B is Boltzmann's constant ($1.38065 \times 10^{-23} \text{ J}\cdot\text{K}^{-1}$), T is temperature (298.15 K), h is Planck's constant ($6.62608 \times 10^{-34} \text{ J}\cdot\text{s}$), R is ideal gas constant ($8.31447 \text{ J}\cdot\text{K}^{-1}\cdot\text{mol}^{-1}$ and $8.20574 \times 10^{-2} \text{ L}\cdot\text{atm}\cdot\text{K}^{-1}\cdot\text{mol}^{-1}$), P_0 is pressure (1 atm), ΔG^\ddagger is the calculated Gibbs free energy of activation [90].

Kinetic and thermodynamic parameters of modelled reactions (Figure 4.5), calculated with B3LYP/6-31+G(d,p) for S: 6-311++G(3df,3pd) in DMF, are given in Table 4.13 which includes the activation energy (ΔG^\ddagger) in kcal/mol, imaginary frequency (ν) of transition state in cm^{-1} , rate constant (k) in $L.mol^{-1}.s^{-1}$, C-C distance in transition state ($d(C-C)$) in Å, overall reaction enthalpy (ΔH_{rxn}^o) in kcal/mol and overall Gibbs free energy (ΔG_{rxn}^o) in kcal/mol.

Table 4.13. Kinetic and thermodynamic parameters of exocyclic and endocyclic radical attack reactions of thioxanthone and phenyl acetic acid derivatives.

Molecule	ΔG^\ddagger	ν	k	$d(C-C)$	Overall	
					ΔH_{rxn}^o	ΔG_{rxn}^o
TX-AA_{exo}	18.72	-425.70	2.88	2.27	-13.62	-2.28
TX-NH-AA_{exo}	15.30	-204.00	9.27 x 10 ²	2.41	-16.50	-4.14
TX-O-AA_{exo}	15.60	-228.33	5.58 x 10 ²	2.44	-24.28	-11.41
TX-S-AA_{exo}	17.92	-324.68	11.1	2.34	-18.97	-6.40
TX-AA_{endo}	27.50	-513.59	1.06 x 10 ⁻⁶	2.11	2.40	16.41
TX-NH-AA_{endo}	27.13	-503.47	1.97 x 10 ⁻⁶	2.10	2.43	16.39
TX-O-AA_{endo}	27.50	-507.82	1.06 x 10 ⁻⁶	2.11	2.50	15.80
TX-S-AA_{endo}	27.57	-512.65	9.39 x 10 ⁻⁷	2.12	2.41	16.60
PHC_{exo}	18.61	-416.50	3.47	2.27	-13.76	-2.53
PHN_{exo}	14.86	-185.44	1.95 x 10 ³	2.43	-16.49	-4.81
PHO_{exo}	14.92	-219.48	1.76 x 10 ³	2.44	-23.84	-11.83
PHS_{exo}	17.86	-314.67	12.3	2.35	-18.96	-7.54
TX_{endo}	27.20	-513.33	1.75 x 10 ⁻⁶	2.11	2.32	16.39

As it can be seen in Table 4.13, TX-AA_{exo}, TX-NH-AA_{exo}, TX-O-AA_{exo}, TX-S-AA_{exo} radical attack to the monomer activation energies are in the range of 15.30 - 18.72 kcal/mol whereas the TX-AA_{endo}, TX-NH-AA_{endo}, TX-O-AA_{endo}, TX-S-AA_{endo} radical attack to the monomer activation energies are in the range of 27.13 - 27.57 kcal/mol. Overall reaction enthalpies and Gibbs free energies indicate an exergonic reaction behavior for all exocyclic radicals.

Even though experimental studies have proposed that the endocyclic radicals may lead to side product formation in same reaction conditions, activation energy of endocyclic radicals are ≈ 10 kcal/mol higher than the one for exocyclic radicals. Therefore, competition between these radicals are in favor of exocyclic radicals and endocyclic radical attack to monomer is unlikely to occur in the same reaction conditions.

Rate constants of radical attack to monomer reactions of all exocyclic radicals are about 10^7 - 10^8 times greater compared to the endocyclic radicals of the same species. ≈ 10 kcal/mol activation energy difference leads to a huge gap between the rate constants of radical attack to monomer reactions.

Even though, thioxanthone acetic acid derivatives differ from each other by the presence of NH group, O and S atom, their endocyclic radicals show similar properties whereas their exocyclic radicals differ from each other in terms of kinetic and thermodynamic parameters. Kinetic and thermodynamic parameters of TX_{endo} radical that forms in the *Type II* photoinitiation system with phenyl acetic acid derivatives also must be considered to make comparisons. In contrast to the endocyclic radicals of thioxanthone acetic acid derivatives, there is no side group attached to the thioxanthone core but TX_{endo} radical also shows similar properties with the endocyclic radicals of thioxanthone acetic acid derivatives.

By considering the side group similarities of different thioxanthone based radicals, one can conclude that the side group functionality has no effect on the kinetic and thermodynamic parameters of the endocyclic radicals but has effect on the exocyclic radicals of the thioxanthone acetic acid derivatives.

Potential energy surface (PES) of TX-AA_{exo} radical attack to the MMA (Figure 4.13) represents the same exergonic character of all exocyclic radical reactions whereas the potential energy surface of TX-AA_{endo} radical attack to the MMA (Figure 4.14) represents the same endergonic character of all endocyclic radical reactions.

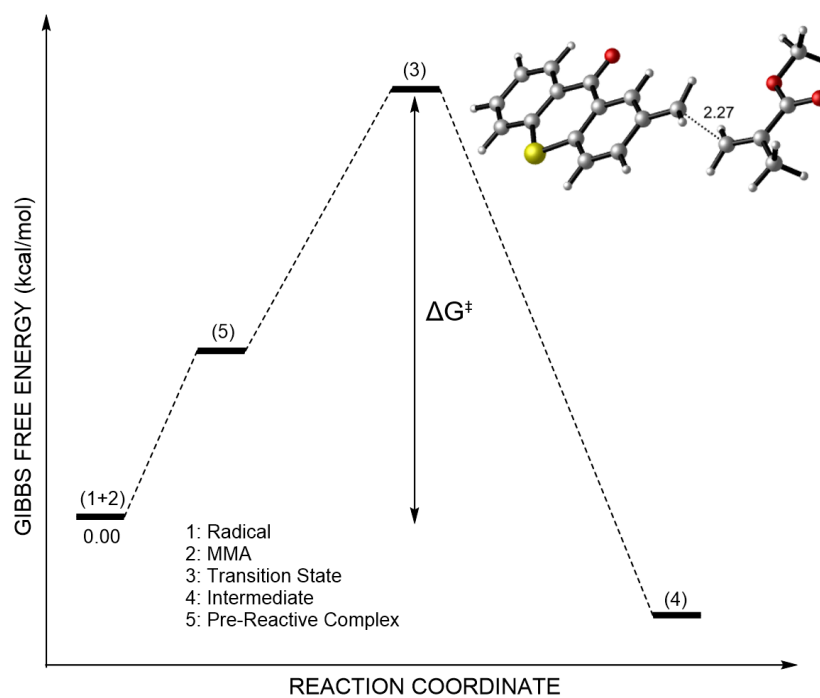


Figure 4.13. PES of TX-AA_{exo} radical attack to MMA.

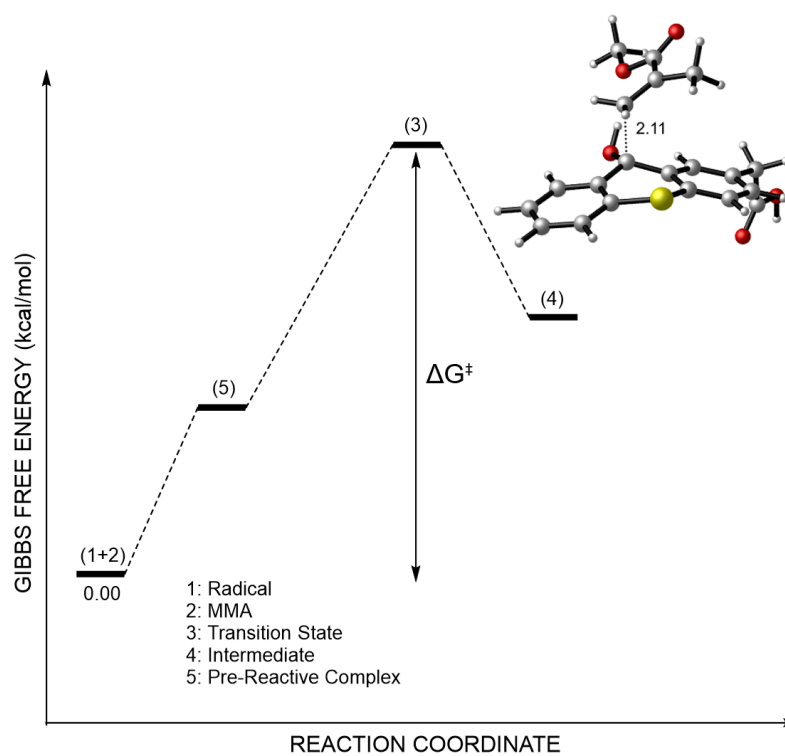


Figure 4.14. PES of TX-AA_{endo} radical attack to MMA.

Spin densities and radical Fukui functions are important parameters which can be useful for assessing the radical reactivity. We have calculated the spin densities and radical Fukui functions of initiating radicals with NPA. Spin densities of the formed radical intermediates after radical attack to monomer have been calculated concurrently (Figure 4.15) (Table 4.14).

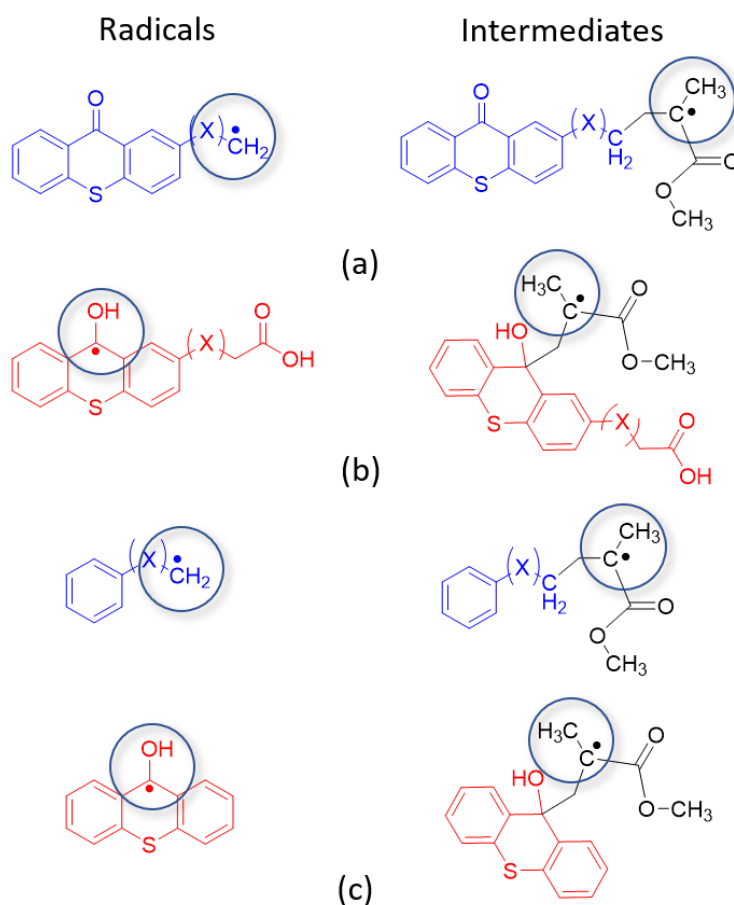


Figure 4.15. Radicalic centers in initiation reactions of (a) and (b) thioxanthone acetic acid derivatives and (c) phenyl acetic acid derivatives.

As it can be seen in Table 4.14, spin densities and radical Fukui function values of exocyclic radicals are similar both for thioxanthone and phenyl acetic acid derivatives. However, spin densities and radical Fukui function values of endocyclic radicals are significantly lower than the exocyclic radicals. It should be also noted that the spin density of the radical, which forms after the endocyclic radical attack (intermediate), is larger than its corresponding endocyclic radical.

Table 4.14. Spin densities and radical Fukui function values of initiating radicals and spin densities of the intermediates calculated with NPA (B3LYP/6-31+G(d,p) for S: 6-311++G(3df,3pd) in DMF).

Molecule	<i>Fukui Function</i>	<i>Spin Density</i>	
	f_k^0	Radical	Intermediate
TX-AA _{exo}	0.354	0.702	0.732
TX-NH-AA _{exo}	0.393	0.760	0.719
TX-O-AA _{exo}	0.454	0.881	0.736
TX-S-AA _{exo}	0.386	0.787	0.734
TX-AA _{endo}	0.197	0.433	0.721
TX-NH-AA _{endo}	0.188	0.422	0.715
TX-O-AA _{endo}	0.190	0.423	0.720
TX-S-AA _{endo}	0.196	0.433	0.723
PHC _{exo}	0.408	0.720	0.730
PHN _{exo}	0.478	0.763	0.714
PHO _{exo}	0.556	0.878	0.732
PHS _{exo}	0.436	0.787	0.730
TX _{endo}	0.197	0.433	0.721

We have carried out regression analyses between the spin densities and radical Fukui function values vs. ΔG^\ddagger (Figure 4.16 to 4.19) to understand whether these findings can be utilized for the determination of the activation energies by only calculating the spin densities and/or the radical Fukui functions of the initiating radicals.

A good correlation have been established between the spin densities and radical Fukui function values vs. ΔG^\ddagger . Including only thioxanthone based radicals have resulted R^2 values of; 0.96 for spin density vs. ΔG^\ddagger (Figure 4.16) and 0.97 for radical Fukui function values vs. ΔG^\ddagger (Figure 4.17). However, including phenyl acetic acid based radicals have resulted slightly lower R^2 values of; 0.95 for spin density vs. ΔG^\ddagger (Figure 4.18) and 0.92 for radical Fukui function values vs. ΔG^\ddagger (Figure 4.19).

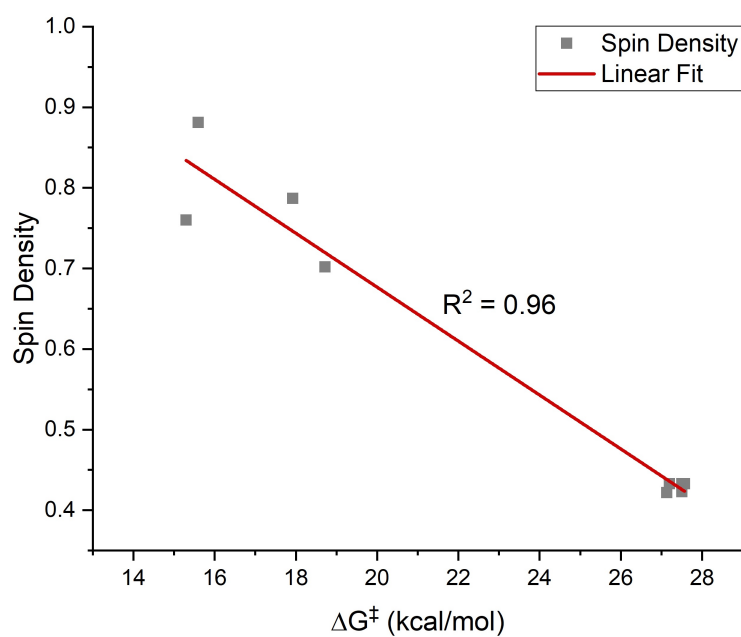


Figure 4.16. Correlation between spin densities and ΔG^\ddagger of thioxanthone based initiating radicals.

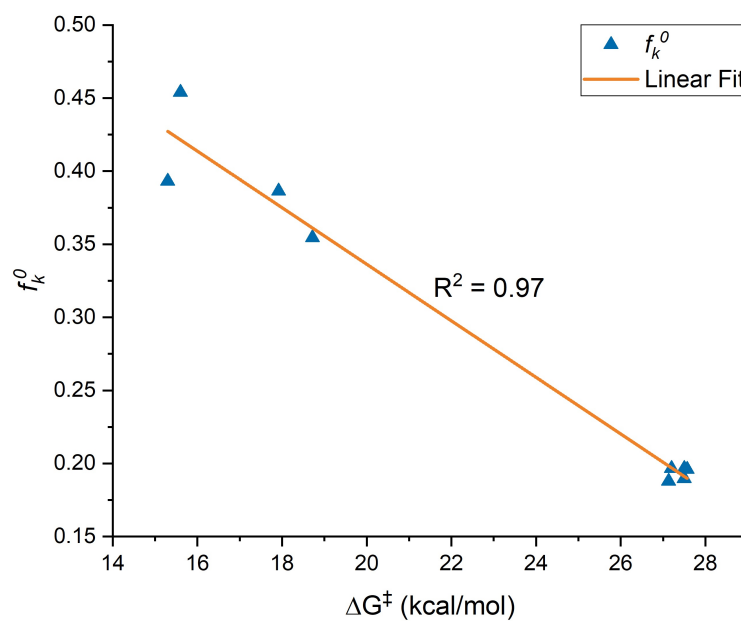


Figure 4.17. Correlation between radical Fukui function and ΔG^\ddagger of thioxanthone based initiating radicals.

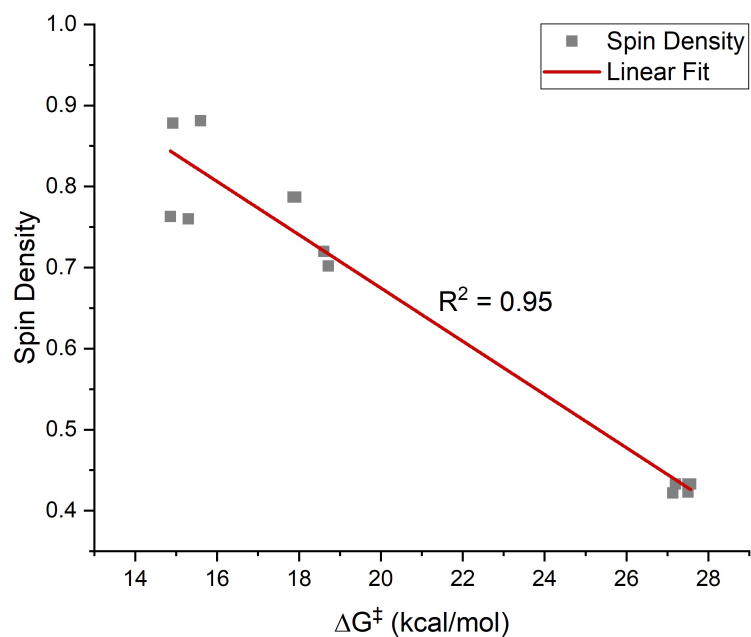


Figure 4.18. Correlation between spin densities and ΔG^\ddagger of thioxanthone and phenyl acetic acid based initiating radicals.

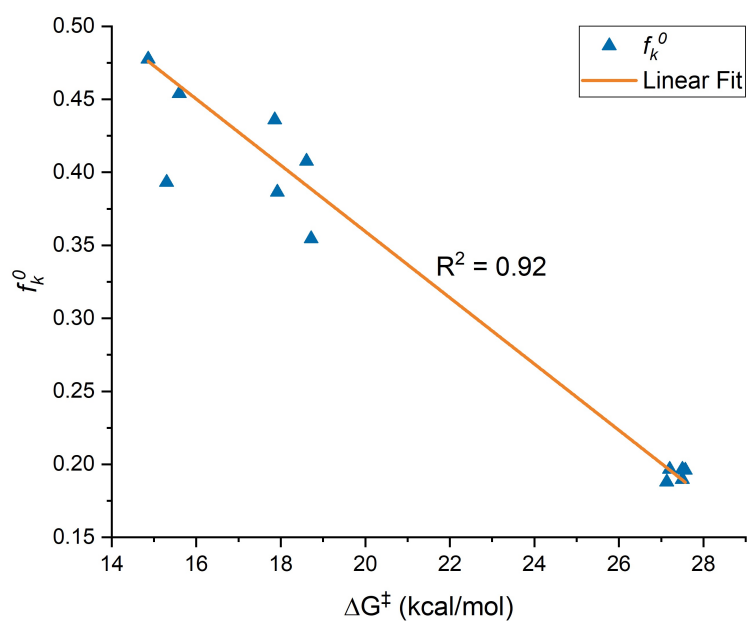


Figure 4.19. Correlation between radical Fukui function and ΔG^\ddagger of thioxanthone and phenyl acetic acid based initiating radicals.

If we look at the overall parameters of initiation reactions, phenyl acetic acid based radicals are in good agreement with the exocyclic thioxanthone acetic acid based radicals. Among the species investigated, differences between the activation energies, rate constants, overall reaction enthalpy and free energy values are minimum. These results indicate that *One-Component Type II* systems have same efficiency with the conventional *Type II* systems in terms of radical attack kinetics and overall thermodynamic parameters.

Photophysical advantages of thioxanthone acetic acid derivatives such as more capability of light absorption in a wide range of light spectrum and having same kinetic efficiency of radical attack to the monomer, make thioxanthone acetic acid derivatives a good candidate for the replacement of conventional *Type II* systems.

5. CONCLUSION

This study can be described as a theoretical and complementary study for the determination of the photophysical, kinetic and thermodynamic properties of the *One-Component Type II* thioxanthone acetic acid photoinitiators which have been synthesized over many years.

In this study, we have successfully defined the best methodology to represent the thioxanthone based molecules in DFT calculations by assessing the level of theory and generating experimentally-comparable absorption spectra. We propose the usage of B3LYP/6-31+G(d,p) and adding extra basis set (6-311++G(3df,3pd)) for S atom for thioxanthone based molecules. The determined methodology for thioxanthone based molecules could lead to the application of the methodology in different studies where the thioxanthone derivatives are utilized for different purposes.

Competition between exocyclic and endocyclic radicals of thioxanthone acetic acid derivatives have been investigated in terms of kinetic and thermodynamic parameters. It has been found that the difference between the exocyclic radical attack and endocyclic radical attack to monomer activation energy is significant in the same reaction conditions. Thus, the radical attack of exocyclic radical is favorable in each modelled reaction. This finding also supports the proposal of Arsu *et al.* where they have proposed that exocyclic radicals are responsible for the initiation of the polymerization reactions.

We were also able to compare the *One-Component Type II* and conventional *Type II* systems. We have observed similar activation energies, exergonic reaction behaviors, spin densities and radical Fukui function values of the radicals in the initiation reactions. For this reason, we believe that *One-Component Type II* photoinitiators can be as effective as the conventional *Type II* photoinitiators.

Regression analyses have suggested a predictive approach for the determination of the activation energies by only calculating the spin density and/or the radical Fukui function of the initiating radicals.

Once and for all, we believe that we have successfully proposed a stepwise approach for the determination of the initiation efficiency of thioxanthone acetic acid based *One-Component Type II* photoinitiators and this approach can be utilized in computational calculations before moving to wet-lab experiments since the available chemical knowledge related to the overall performance of a designed photoinitiator could save energy and resources.

REFERENCES

1. Cinar, S. A., M. N. Guven, T. N. Eren, B. Cesur, M. Aleksanyan, B. Dedeoglu, N. Okte, V. Aviyente, F. Morlet-Savary, J. Lalevée and D. Avci, “Structure-reactivity relationships of novel monomeric photoinitiators”, *Journal of Photochemistry and Photobiology A: Chemistry*, Vol. 329, pp. 77–87, 2016.
2. Furuncuoğlu, T., I. Uğur, I. Degirmenci and V. Aviyente, “Role of chain transfer agents in free radical polymerization kinetics”, *Macromolecules*, Vol. 43, No. 4, pp. 1823–1835, 2010.
3. Degirmenci, I. and M. L. Coote, “Effect of Substituents on the Stability of Sulfur-Centered Radicals”, *Journal of Physical Chemistry A*, Vol. 120, No. 37, pp. 7398–7403, 2016.
4. Fouassier, J. P., D. Rinaldi, X. Allonas, J. Lalevée, M. F. Ruiz Lopez and J. L. Rivail, “Solvent effect on the radical addition reaction to double bond: Experimental and quantum chemical investigations”, *Chemical Physics Letters*, Vol. 415, No. 4-6, pp. 202–205, 2005.
5. Lalevée, J., D. Gigmes, D. Bertin, B. Graff, X. Allonas and J. P. Fouassier, “Comparative reactivity of aminyl and aminoalkyl radicals”, *Chemical Physics Letters*, Vol. 438, No. 4-6, pp. 346–350, 2007.
6. Degirmenci, I. and M. L. Coote, “Comparison of Thiyl, Alkoxy, and Alkyl Radical Addition to Double Bonds: The Unusual Contrasting Behavior of Sulfur and Oxygen Radical Chemistry”, *Journal of Physical Chemistry A*, Vol. 120, No. 10, pp. 1750–1755, 2016.
7. Lalevée, J., X. Allonas and J. P. Fouassier, “Halogen abstraction reaction between aminoalkyl radicals and alkyl halides: Unusual high rate constants”, *Chemical Physics Letters*, Vol. 454, No. 4-6, pp. 415–418, 2008.

8. Özaltın, T. F., S. Catak, B. Kiskan, Y. Yagci and V. Aviyente, “Rationalizing the regioselectivity of cationic ring-opening polymerization of benzoxazines”, *European Polymer Journal*, Vol. 105, pp. 61–67, 2018.
9. Dogan, B., S. Catak, V. V. Speybroeck, M. Waroquier and V. Aviyente, “Free radical polymerization of ethyl methacrylate and ethyl α -hydroxy methacrylate: A computational approach to the propagation kinetics”, *Polymer*, Vol. 53, No. 15, pp. 3211–3219, 2012.
10. Fouassier, J. P. and J. Lalevée, *Photoinitiators for Polymer Synthesis*, Wiley VCH Verlag GmbH & Co. KGaA, Weinheim, 2012.
11. Yagci, Y., S. Jockusch and N. J. Turro, “Photoinitiated polymerization: Advances, challenges, and opportunities”, *Macromolecules*, Vol. 43, No. 15, pp. 6245–6260, 2010.
12. Ito, Y., *Photochemistry for Biomedical Applications*, Springer, 2018.
13. Mishra, M. and Y. Yagci, *Handbook of Vinyl Polymers: Radical Polymerization, Process, and Technology, Second Edition*, Plastics Engineering, Taylor & Francis, 2008.
14. Albini, A., *Photochemistry: Past, Present and Future*, Springer, 2015.
15. Wardle, B., *Principles and Applications of Photochemistry*, Wiley, 2009.
16. Allen, N. S., *Photochemistry and Photophysics of Polymer Materials*, John Wiley & Sons, Inc., 2010.
17. Fouassier, J. P., X. Allonas, J. Lalevée and C. Dietlin, “Photoinitiators for Free Radical Polymerization Reactions”, *Photochemistry and Photophysics of Polymer Materials*, chap. 10, pp. 351–419, John Wiley & Sons, Inc., 2010.
18. Turro, N. J., V. Ramamurthy, V. Ramamurthy and J. C. Scaiano, *Principles of*

- Molecular Photochemistry: An Introduction*, Raymond F. Boyer Library Collection, University Science Books, 2009.
19. Ramamurthy, V. and K. S. Schanze, *Organic Photochemistry and Photophysics*, Molecular and Supramolecular Photochemistry, Taylor & Francis, 2005.
 20. Balzani, V., P. Ceroni and A. Juris, *Photochemistry and Photophysics: Concepts, Research, Applications*, Wiley, 2014.
 21. Dietliker, K. and J. Baro, “Photoinitiators”, *Handbook of Industrial Inkjet Printing: A Full System Approach*, chap. 4, pp. 59–116, Wiley, 2017.
 22. Palmeira, A., M. H. Vasconcelos, A. Paiva, M. X. Fernandes, M. Pinto and E. Sousa, “Dual inhibitors of P-glycoprotein and tumor cell growth: (Re) discovering thioxanthenes”, *Biochemical Pharmacology*, Vol. 83, No. 1, pp. 57–68, 2012.
 23. Arsu, N., M. Aydin, Y. Yagci, S. Jockusch and N. J. Turro, “One component thioxanthone based Type II photoinitiators”, *Photochemistry and UV Curing: New Trends*, Vol. 661, No. 2, pp. 1–13, 2006.
 24. Metin, E., G. S. Batibay and N. Arsu, “In-situ formation of self-assembled Ag nanoclusters on ct-DNA in the presence of 2-mercaptothioxanthone by using UV-vis light irradiation”, *Journal of Photochemistry and Photobiology A: Chemistry*, Vol. 356, pp. 1–6, 2018.
 25. Kreutzer, J., K. Kaya and Y. Yagci, “Poly(propylene oxide)-thioxanthone as one-component Type II polymeric photoinitiator for free radical polymerization with low migration behavior”, *European Polymer Journal*, Vol. 99, No. June, pp. 528–532, 2018.
 26. Karaca, N., N. Ocal, N. Arsu and S. Jockusch, “Thioxanthone-benzothiophenes as photoinitiator for free radical polymerization”, *Journal of Photochemistry and*

- Photobiology A: Chemistry*, Vol. 331, pp. 22–28, 2016.
27. Dadashi-Silab, S., C. Aydogan and Y. Yagci, “Shining a light on an adaptable photoinitiator: advances in photopolymerizations initiated by thioxanthenes”, *Polymer Chemistry*, Vol. 6, No. 37, pp. 6595–6615, 2015.
 28. Wang, L., A. Cavaco-Paulo, B. Xu and M. Martins, “Humidity induces changes in the dimensions of hydrogel-coated wool yarns”, *Polymers*, Vol. 10, No. 260, pp. 1–12, 2018.
 29. Cokbaglan, L., N. Arsu, Y. Yagci, S. Jockusch and N. J. Turro, “2-Mercaptothioxanthone As a Novel Photoinitiator for Free Radical Polymerization”, *Macromolecules*, Vol. 36, No. 8, pp. 2649–2653, 2003.
 30. Wu, Q., Y. Xiong, Q. Liang and H. Tang, “Developing thioxanthone based visible photoinitiators for radical polymerization”, *RSC Advances*, Vol. 4, No. 94, pp. 52324–52331, 2014.
 31. Qiu, J. and J. Wei, “Thioxanthone photoinitiator containing polymerizable N-aromatic maleimide for photopolymerization”, *Journal of Polymer Research*, Vol. 21, No. 9, 2014.
 32. Kreutzer, J. and Y. Yagci, “One-component, double-chromophoric thioxanthone photoinitiators for free radical polymerization”, *Journal of Polymer Science, Part A: Polymer Chemistry*, Vol. 55, No. 20, pp. 3475–3482, 2017.
 33. Eren, T. N., N. Yasar, V. Aviyente, F. Morlet-Savary, B. Graff, J. P. Fouassier, J. Lalevee and D. Avci, “Photophysical and Photochemical Studies of Novel Thioxanthone-Functionalized Methacrylates through LED Excitation”, *Macromolecular Chemistry and Physics*, Vol. 217, No. 13, pp. 1501–1512, 2016.
 34. Lalevée, J., N. Blanchard, M. Ali Tehfe, C. Fries, F. Morlet-Savary, D. Gigmes and J. P. Fouassier, “New thioxanthone and xanthone photoinitiators based on silyl

- radical chemistry”, *Polymer Chemistry*, Vol. 2, No. 5, pp. 1077–1084, 2011.
35. Esen, D. S., G. Temel, D. K. Balta, X. Allonas and N. Arsu, “One-component thioxanthone acetic acid derivative photoinitiator for free radical polymerization”, *Photochemistry and Photobiology*, Vol. 90, No. 2, pp. 463–469, 2014.
 36. Tar, H., D. Sevinc Esen, M. Aydin, C. Ley, N. Arsu and X. Allonas, “Panchromatic type II photoinitiator for free radical polymerization based on thioxanthone derivative”, *Macromolecules*, Vol. 46, No. 9, pp. 3266–3272, 2013.
 37. Aydin, M., N. Arsu and Y. Yagci, “One-component bimolecular photoinitiating systems, 2a: Thioxanthone acetic acid derivatives as photoinitiators for free radical polymerization”, *Macromolecular Rapid Communications*, Vol. 24, No. 12, pp. 718–723, 2003.
 38. Karasu, F., M. Aydin, M. A. Kaya, D. K. Balta and N. Arsu, “Determination of photoinitiated polymerization of multifunctional acrylates with acetic acid derivatives of thioxanthone by RT-FTIR”, *Progress in Organic Coatings*, Vol. 64, No. 1, pp. 1–4, 2009.
 39. Çeper, T. and N. Arsu, “Photochemically Prepared Gold/Polymer Nanocoatings: Formation of Gold Mirror”, *Macromolecular Chemistry and Physics*, Vol. 218, No. 18, pp. 1–8, 2017.
 40. Ataci, N. and N. Arsu, “Studies of the binding mode of TXNHCH₂COOH with calf thymus DNA by spectroscopic methods”, *Spectrochimica Acta - Part A: Molecular and Biomolecular Spectroscopy*, Vol. 169, pp. 128–133, 2016.
 41. Batibay, G. S., O. T. Gunkara, N. Ocal and N. Arsu, “In-situ photoinduced formation of self-assembled Ag NPs using POSS-TX as nano-photoinitiator in PEG-MEA/PEGDA polymer matrix and creating self-wrinkled pattern”, *Journal of Photochemistry and Photobiology A: Chemistry*, Vol. 359, pp. 73–79, 2018.

42. Wang, Z., Y. Li, X. Cai, D. Chen, G. Xie, K. K. Liu, Y. C. Wu, C. C. Lo, A. Lien, Y. Cao and S. J. Su, "Structure-Performance Investigation of Thioxanthone Derivatives for Developing Color Tunable Highly Efficient Thermally Activated Delayed Fluorescence Emitters", *ACS Applied Materials and Interfaces*, Vol. 8, No. 13, pp. 8627–8636, 2016.
43. Li, Y., X. L. Li, D. Chen, X. Cai, G. Xie, Z. He, Y. C. Wu, A. Lien, Y. Cao and S. J. Su, "Design Strategy of Blue and Yellow Thermally Activated Delayed Fluorescence Emitters and Their All-Fluorescence White OLEDs with External Quantum Efficiency beyond 20%", *Advanced Functional Materials*, Vol. 26, No. 38, pp. 6904–6912, 2016.
44. Sun, H., Z. Hu, C. Zhong, X. Chen, Z. Sun and J. L. Brédas, "Impact of Dielectric Constant on the Singlet-Triplet Gap in Thermally Activated Delayed Fluorescence Materials", *Journal of Physical Chemistry Letters*, Vol. 8, No. 11, pp. 2393–2398, 2017.
45. Beni, A. S., A. N. Chermahini, H. Sharghi and S. M. Monfared, "MP2, DFT and ab initio calculations on thioxanthone", *Spectrochimica Acta - Part A: Molecular and Biomolecular Spectroscopy*, Vol. 82, No. 1, pp. 49–55, 2011.
46. Beni, A. S. and S. M. Monfared, "DFT and MP2 calculations on new series of hydroxythioxanthones", *Journal of Molecular Structure*, Vol. 1039, pp. 8–21, 2013.
47. Leggesse, E. G., W. R. Tong, S. Nachimuthu, T. Y. Chen and J. C. Jiang, "Theoretical study on photochemistry of Irgacure 907", *Journal of Photochemistry and Photobiology A: Chemistry*, Vol. 347, pp. 78–85, 2017.
48. Fast, D. E., A. Lauer, J. P. Menzel, A. M. Kelterer, G. Gescheidt and C. Barner-Kowollik, "Wavelength-Dependent Photochemistry of Oxime Ester Photoinitiators", *Macromolecules*, Vol. 50, No. 5, pp. 1815–1823, 2017.
49. Loeb, A. L., "The Heisenberg Uncertainty Principle", *American Journal of*

- Physics*, Vol. 31, No. 12, p. 945, 1963.
50. Born, M. and R. Oppenheimer, “Zur Quantentheorie der Molekeln”, *Annalen der Physik*, Vol. 389, No. 20, pp. 457–484, 1927.
 51. Engel, E. and R. M. Dreizler, *Density Functional Theory: An Advanced Course*, Theoretical and Mathematical Physics, Springer, 2011.
 52. Becke, A. D., “A new mixing of Hartree-Fock and local density-functional theories”, *The Journal of Chemical Physics*, Vol. 98, No. 2, pp. 1372–1377, 1993.
 53. Becke, A. D., “Density-functional exchange approximation with correct asymptotic behaviour”, *Physical Review A*, Vol. 38, No. 6, pp. 3098–3100, 1988.
 54. Hohenberg, P. and W. Kohn, “Inhomogeneous electron gas”, *Physical Review*, Vol. 136, pp. B864–B871, 1964.
 55. Kohn, W. and L. J. Sham, “Self-consistent equations including exchange and correlation effects”, *Physical Review*, Vol. 140, No. 4A, pp. A1133–A1138, 1965.
 56. Leach, A. R., *Molecular Modelling: Principles and Applications*, Prentice Hall, 2001.
 57. Perdew, J. P., K. Burke and M. Ernzerhof, “Generalized gradient approximation made simple”, *Physical Review Letters*, Vol. 77, No. 18, pp. 3865–3868, 1996.
 58. Lee, C., W. Yang and R. G. Parr, “Development of the Colle-Salvetti correlation-energy formula into a functional of the electron density”, *Physical Review B*, Vol. 37, No. 2, pp. 785–789, 1988.
 59. Pauling, L., “The nature of the chemical bond. IV. The energy of single bonds and the relative electronegativity of atoms”, *Journal of the American Chemical Society*, Vol. 54, No. 9, pp. 3570–3582, 1932.

60. Zhao, Y. and D. G. Truhlar, “The M06 suite of density functionals for main group thermochemistry, thermochemical kinetics, noncovalent interactions, excited states, and transition elements: Two new functionals and systematic testing of four M06-class functionals and 12 other function”, *Theoretical Chemistry Accounts*, Vol. 120, No. 1-3, pp. 215–241, 2008.
61. Chai, J. D. and M. Head-Gordon, “Long-range corrected hybrid density functionals with damped atom-atom dispersion corrections”, *Physical Chemistry Chemical Physics*, Vol. 10, No. 44, pp. 6615–6620, 2008.
62. Vydrov, O. A. and G. E. Scuseria, “Assessment of a long-range corrected hybrid functional”, *J. Chem. Phys.*, Vol. 125, No. 23, p. 234109, 2006.
63. Slater, J. C., “Atomic Shielding Constants”, *Phys. Rev.*, Vol. 36, No. 1, pp. 57–64, 1930.
64. Boys, S. F. and A. C. Egerton, “Electronic wave functions - I. A general method of calculation for the stationary states of any molecular system”, *Proceedings of the Royal Society of London. Series A. Mathematical and Physical Sciences*, Vol. 200, No. 1063, pp. 542–554, 1950.
65. Runge, E. and E. K. U. Gross, “Density-Functional Theory for Time-Dependent Systems”, *Phys. Rev. Lett.*, Vol. 52, No. 12, pp. 997–1000, 1984.
66. Miertuš, S., E. Scrocco and J. Tomasi, “Electrostatic interaction of a solute with a continuum. A direct utilization of AB initio molecular potentials for the prevision of solvent effects”, *Chemical Physics*, Vol. 55, No. 1, pp. 117–129, 1981.
67. Wigner, E. P., “On the Quantum Correction for Thermodynamic Equilibrium”, *Part I: Physical Chemistry. Part II: Solid State Physics*, pp. 110–120, Springer Berlin Heidelberg, Berlin, Heidelberg, 1997.
68. Steuernagel, O., D. Kakofengitis and G. Ritter, “Wigner Flow Reveals Topological

- Order in Quantum Phase Space Dynamics”, *Phys. Rev. Lett.*, Vol. 110, No. 3, p. 30401, 2013.
69. Etienne, T., X. Assfeld and A. Monari, “New insight into the topology of excited states through detachment/attachment density matrices-based centroids of charge”, *J. Chem. Theory Comput.*, Vol. 10, No. 9, pp. 3906–3914, 2014.
70. Etienne, T., X. Assfeld and A. Monari, “Toward a quantitative assessment of electronic transitions” charge-transfer character”, *J. Chem. Theory Comput.*, Vol. 10, No. 9, pp. 3896–3905, 2014.
71. Etienne, T., “Probing the Locality of Excited States with Linear Algebra”, *J. Chem. Theory Comput.*, Vol. 11, No. 4, pp. 1692–1699, 2015.
72. Ma, Y., J. Liang, D. Zhao, Y. L. Chen, J. Shen and B. Xiong, “Condensed Fukui function predicts innate C-H radical functionalization sites on multi-nitrogen containing fused arenes”, *RSC Advances*, Vol. 4, No. 33, pp. 17262–17264, 2014.
73. Huizar, L. H., C. H. Rios-Reyes, N. J. Olvera-Maturano, J. Robles and J. A. Rodriguez, “Chemical reactivity of quinclorac employing the HSAB local principle - Fukui function”, *Open Chemistry*, Vol. 13, No. 1, pp. 52–60, 2015.
74. Bendjeddou, A., T. Abbaz, A. Gouasmia and D. Villemin, “Molecular Structure, HOMO-LUMO, MEP and Fukui Function Analysis of Some TTF-donor Substituted Molecules Using DFT (B3LYP) Calculations”, *International Research Journal of Pure and Applied Chemistry*, Vol. 12, No. 1, pp. 1–9, 2016.
75. Domingo, L. R., M. Ríos-Gutiérrez and P. Pérez, “Applications of the conceptual density functional theory indices to organic chemistry reactivity”, *Molecules*, Vol. 21, No. 6, 2016.
76. Parr, R. G. and W. Yang, “Density functional approach to the frontier-electron theory of chemical reactivity”, *Journal of the American Chemical Society*, Vol.

- 106, No. 14, pp. 4049–4050, 1984.
77. M. J. Frisch, G. Trucks, H. B. Schlegel, G. E. Scuseria, M. A. Robb, J. R. Cheeseman, G. Scalmani, V. Barone, B. Mennucci, G. A. Petersson *et al.*, “Gaussian 09 Revision E.01”, *Gaussian Inc. Wallingford CT.*, 2013.
78. Hanwell, M. D., D. E. Curtis, D. C. Lonie, T. Vandermeersch, E. Zurek and G. R. Hutchison, “Avogadro: an advanced semantic chemical editor, visualization, and analysis platform”, *Journal of Cheminformatics*, Vol. 4, No. 1, pp. 1–17, 2012.
79. Barbatti, M., M. Ruckebauer, F. Plasser, J. Pittner, G. Granucci, M. Persico and H. Lischka, “Newton-X: A surface-hopping program for nonadiabatic molecular dynamics”, *Wiley Interdisciplinary Reviews: Computational Molecular Science*, Vol. 4, No. 1, pp. 26–33, 2014.
80. Chen, Y.-C., Y.-T. Kuo and T.-H. Ho, “Photo-polymerization properties of type-II photoinitiator systems based on 2-chlorohexaaryl biimidazole (o-Cl-HABI) and various N-phenylglycine (NPG) derivatives”, *Photochemical & Photobiological Sciences*, Vol. 18, No. 1, pp. 190–197, 2019.
81. Al Mousawi, A., P. Garra, M. Schmitt, J. Toufaily, T. Hamieh, B. Graff, J. P. Fouassier, F. Dumur and J. Lalevée, “3-Hydroxyflavone and N-Phenylglycine in High Performance Photoinitiating Systems for 3D Printing and Photocomposites Synthesis”, *Macromolecules*, Vol. 51, No. 12, pp. 4633–4641, 2018.
82. Zhang, J., J. Lalevée, X. Mou, F. Morlet-Savary, B. Graff and P. Xiao, “N-Phenylglycine as a Versatile Photoinitiator under Near-UV LED”, *Macromolecules*, Vol. 51, No. 10, pp. 3767–3773, 2018.
83. Takahashi, H., Y. Marushima, K. Tsuji, K. Shibuya and A. Kawai, “Addition Rate Constants of Phosphorus- and Carbon-Centered Radicals to Double Bond of Monomers as Studied by a Pulsed Electron Paramagnetic Resonance Method.”, *Journal of Physical Chemistry A*, Vol. 119, No. 30, pp. 8261–8268, 2015.

84. Allonas, X., J. Lalevée, F. Morlet-Savary and J. P. Fouassier, “Understanding the reactivity of photoinitiating systems for photopolymerization”, *Polimery/Polymers*, Vol. 51, No. 7, pp. 491–498, 2006.
85. Lalevée, J., X. Allonas and J. P. Fouassier, “Prediction of initiation efficiency in radical photopolymerization: The case of benzoyl and isopropylketyl radicals”, *Macromolecules*, Vol. 38, No. 10, pp. 4521–4524, 2005.
86. Sengul, O., M. Marazzi, A. Monari and S. Catak, “Photophysical Properties of Novel Two-Photon Absorbing Dyes: Assessing Their Possible Use for Singlet Oxygen Generation”, *J. Phys. Chem. C*, Vol. 122, No. 28, pp. 16315–16324, 2018.
87. García-Iriepa, C. and M. Marazzi, “Level of theory and solvent effects on DASA absorption properties prediction: Comparing TD-DFT, CASPT2 and NEVPT2”, *Materials*, Vol. 10, No. 9, pp. 1–13, 2017.
88. Gattuso, H., A. Monari and M. Marazzi, “Photophysics of chlorin e6: from one- and two-photon absorption to fluorescence and phosphorescence”, *RSC Advances*, Vol. 7, No. 18, pp. 10992–10999, 2017.
89. Gattuso, H., E. Dumont, M. Marazzi and A. Monari, “Two-photon-absorption DNA sensitization: Via solvated electron production: Unraveling photochemical pathways by molecular modeling and simulation”, *Physical Chemistry Chemical Physics*, Vol. 18, No. 27, pp. 18598–18606, 2016.
90. Atkins, P. and J. De Paula, *Atkins’s Physical Chemistry*, Oxford University Press, New York, 9 edn., 2010.

APPENDIX A: GROUND STATE GEOMETRIES

Optimization calculations have been carried out with B3LYP/6-31+G(d,p) for S: 6-311++G(3df,3pd) in DMF. After preparing the initial input of the structure, preliminary optimization calculations have been carried out accordingly. 360° dihedral scan calculations (12 steps with 30°) have been conducted on the initially optimized structures for all possible rotations of the bonds. After scan calculations, the minimum energy conformers have been selected for further optimization calculations to obtain the final minimum energy conformer.

The approach mentioned above, has been broadened for the transition state structures and the intermediate structures. For transition state and intermediate structures, 360° scan calculations of C-C bond centered dihedral (between the vinylic C of MMA and the radical C of the initiator) have been carried out to check the existence of a possible minimum energy conformer.

In conjunction with the transition state search, intrinsic reaction coordinate (IRC) calculations have been conducted for the verification of the correct transition state structures. Forward and backward IRC calculations have been carried out by the obtained transition state structures. Conformers that were generated in IRC calculations have been retrieved and optimized. Thus, the pre-reactive complex and the intermediate structures have been obtained.

In Tables A.1 to A.4, optimized ground state structures of the initiation reactions of exocyclic radicals of thioxanthone acetic acid derivatives are given. In all exocyclic radical reactions, planar shape of the thioxanthone core has been observed.

Table A.1. Optimized ground state geometries of TX-AA_{exo} radical attack to MMA
(B3LYP/6-31+G(d,p) for S: 6-311++G(3df,3pd) in DMF).

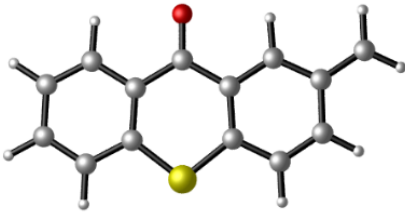
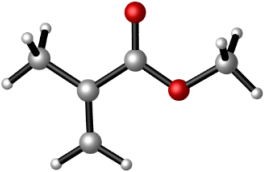
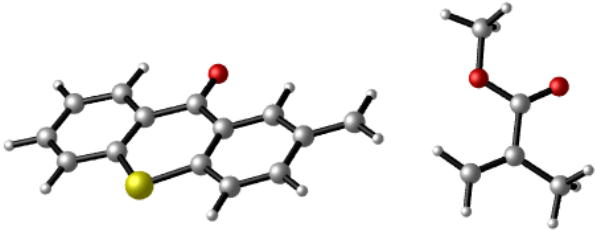
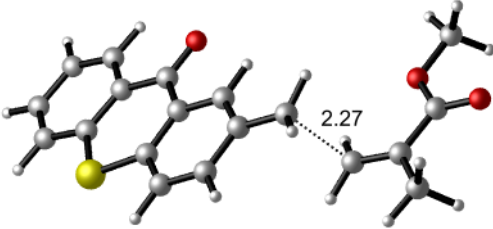
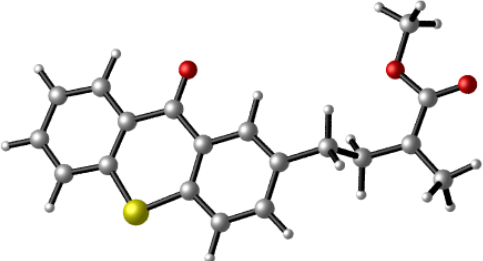
Name	Structure
Reactant 1	
Reactant 2	
Pre-Reactive Complex	
Transition State	
Intermediate	

Table A.2. Optimized ground state geometries of TX-NH-AA_{exo} radical attack to MMA (B3LYP/6-31+G(d,p) for S: 6-311++G(3df,3pd) in DMF).

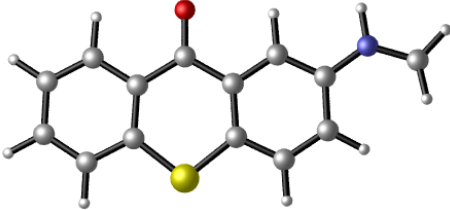
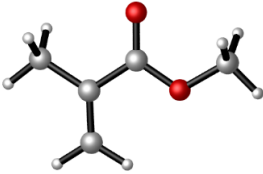
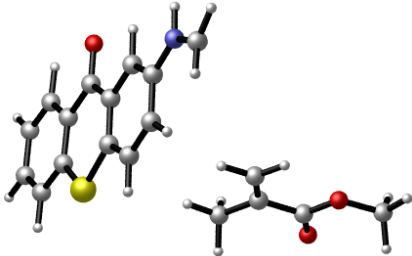
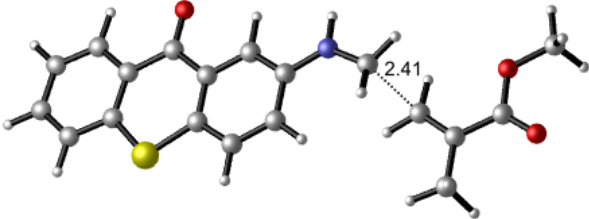
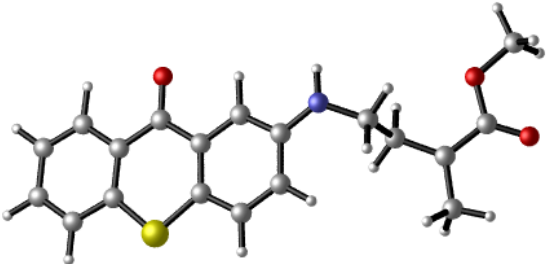
Name	Structure
Reactant 1	
Reactant 2	
Pre-Reactive Complex	
Transition State	
Intermediate	

Table A.3. Optimized ground state geometries of TX-O-AA_{exo} radical attack to MMA (B3LYP/6-31+G(d,p) for S: 6-311++G(3df,3pd) in DMF).

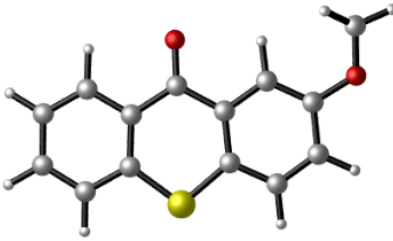
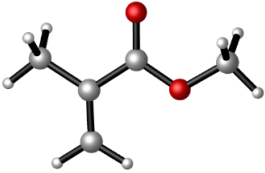
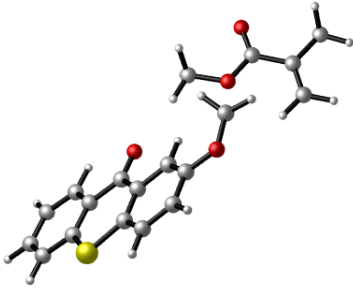
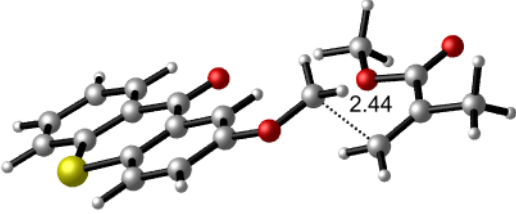
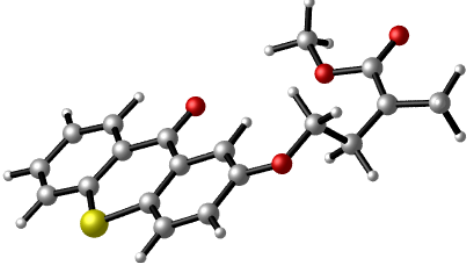
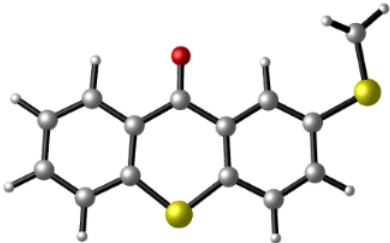
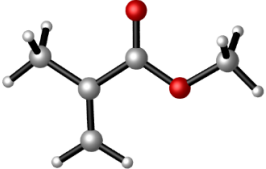
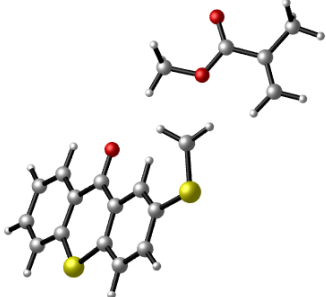
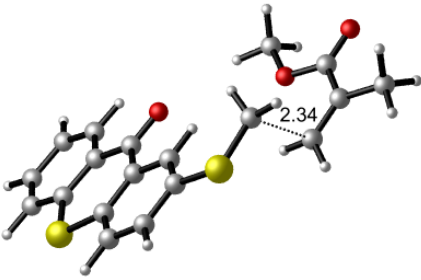
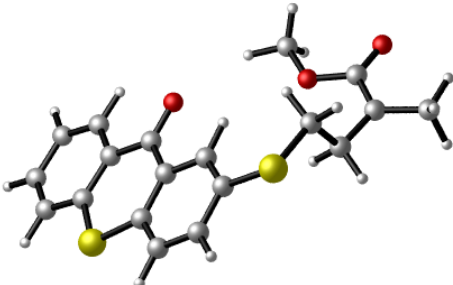
Name	Structure
Reactant 1	
Reactant 2	
Pre-Reactive Complex	
Transition State	
Intermediate	

Table A.4. Optimized ground state geometries of TX-S-AA_{exo} radical attack to MMA (B3LYP/6-31+G(d,p) for S: 6-311++G(3df,3pd) in DMF).

Name	Structure
Reactant 1	
Reactant 2	
Pre-Reactive Complex	
Transition State	
Intermediate	

In the case of endocyclic radical reactions (Table A.5 to A.8), a non-planar bended butterfly shape of the thioxanthone core has been observed. This bending phenomenon has been previously reported also by Beni *et al.* [45].

Table A.5. Optimized ground state geometries of TX-AA_{endo} radical attack to MMA (B3LYP/6-31+G(d,p) for S: 6-311++G(3df,3pd) in DMF).

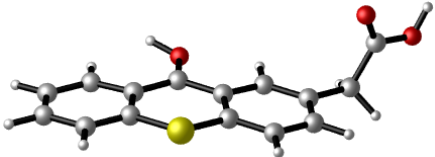
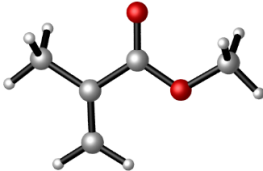
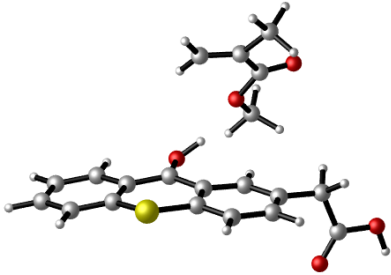
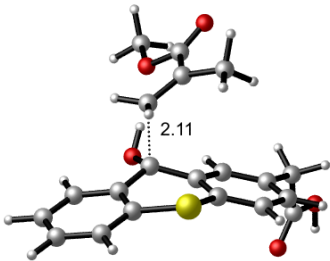
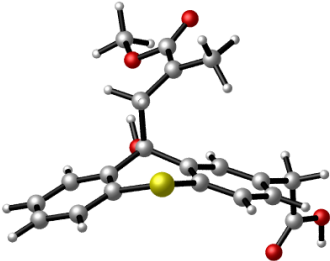
Name	Structure
Reactant 1	
Reactant 2	
Pre-Reactive Complex	
Transition State	
Intermediate	

Table A.6. Optimized ground state geometries of TX-NH-AA_{endo} radical attack to MMA (B3LYP/6-31+G(d,p) for S: 6-311++G(3df,3pd) in DMF).

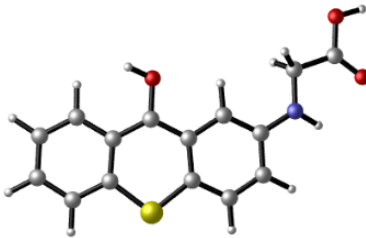
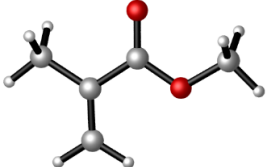
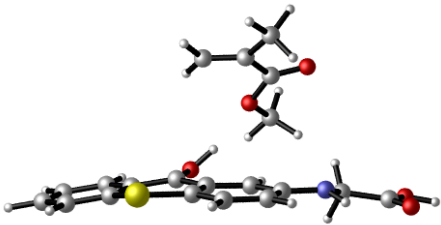
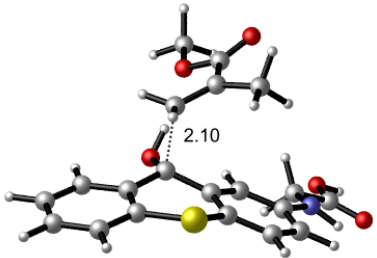
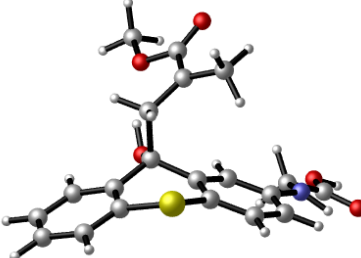
Name	Structure
Reactant 1	
Reactant 2	
Pre-Reactive Complex	
Transition State	
Intermediate	

Table A.7. Optimized ground state geometries of TX-O-AA_{endo} radical attack to MMA (B3LYP/6-31+G(d,p) for S: 6-311++G(3df,3pd) in DMF).

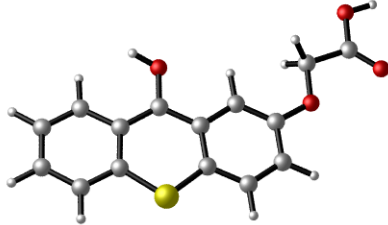
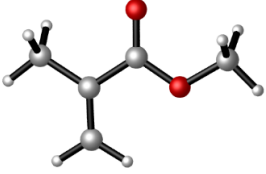
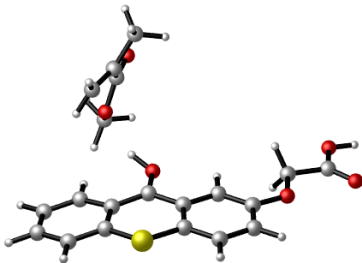
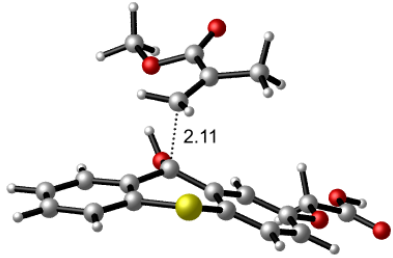
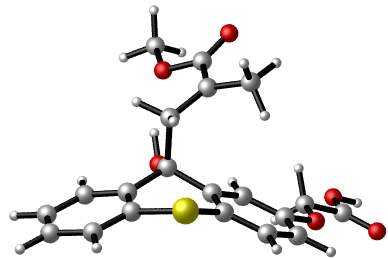
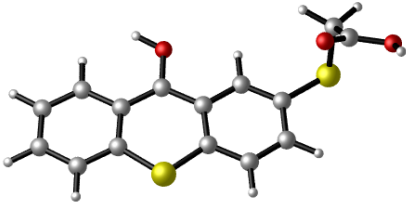
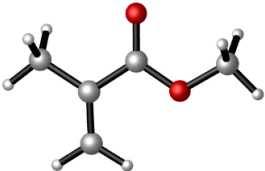
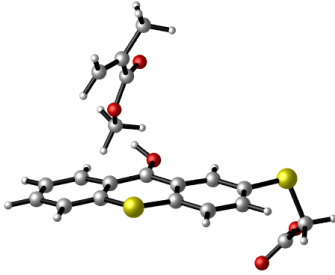
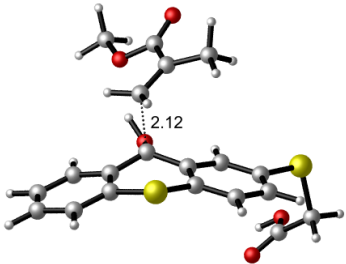
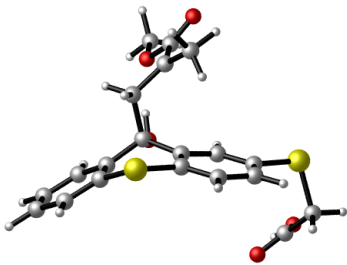
Name	Structure
Reactant 1	
Reactant 2	
Pre-Reactive Complex	
Transition State	
Intermediate	

Table A.8. Optimized ground state geometries of TX-S-AA_{endo} radical attack to MMA (B3LYP/6-31+G(d,p) for S: 6-311++G(3df,3pd) in DMF).

Name	Structure
Reactant 1	
Reactant 2	
Pre-Reactive Complex	
Transition State	
Intermediate	

For the exocyclic radical attack reactions of phenyl acetic acid derivatives, same approach (discussed at the beginning of the appendix) for obtaining the minimum energy conformers have been used. Exocyclic radicals of phenyl acetic acid derivatives have shown a planar shape of the main phenyl cores (Table A.9 to A.12).

Table A.9. Optimized ground state geometries of PHC_{exo} radical attack to MMA (B3LYP/6-31+G(d,p) for S: 6-311++G(3df,3pd) in DMF).

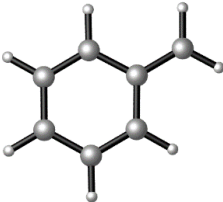
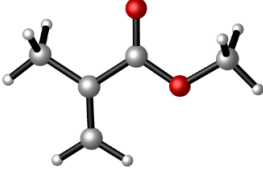
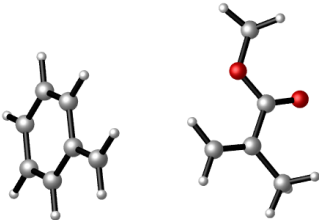
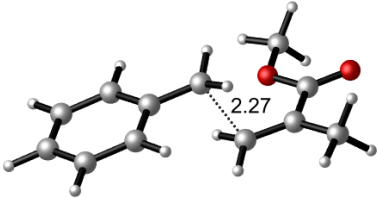
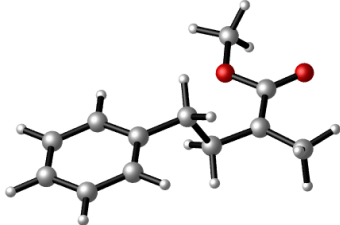
Name	Structure
Reactant 1	
Reactant 2	
Pre-Reactive Complex	
Transition State	
Intermediate	

Table A.10. Optimized ground state geometries of PHN_{exo} radical attack to MMA
(B3LYP/6-31+G(d,p) for S: 6-311++G(3df,3pd) in DMF).

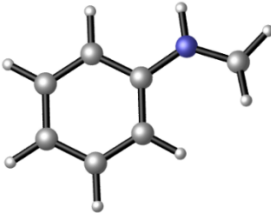
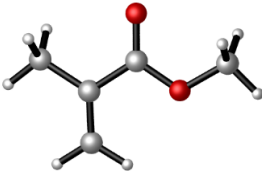
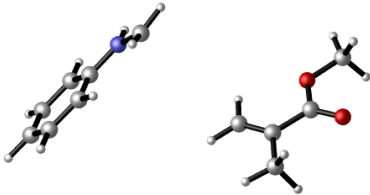
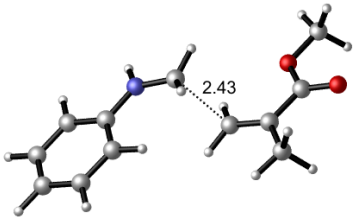
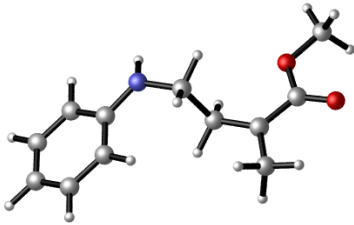
Name	Structure
Reactant 1	
Reactant 2	
Pre-Reactive Complex	
Transition State	
Intermediate	

Table A.11. Optimized ground state geometries of PHO_{exo} radical attack to MMA
(B3LYP/6-31+G(d,p) for S: 6-311++G(3df,3pd) in DMF).

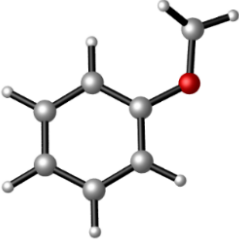
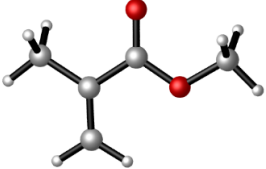
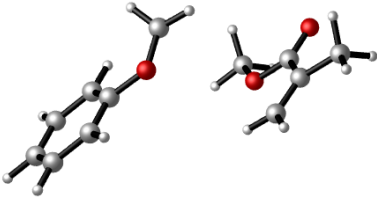
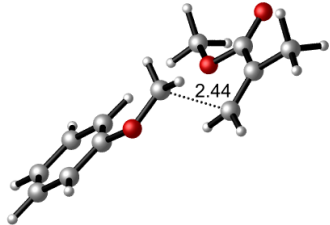
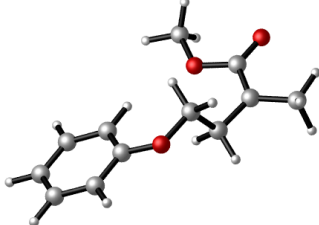
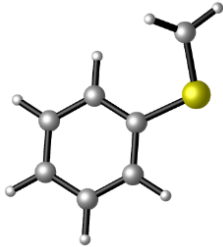
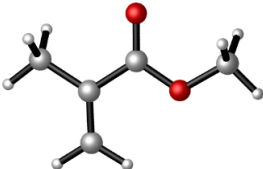
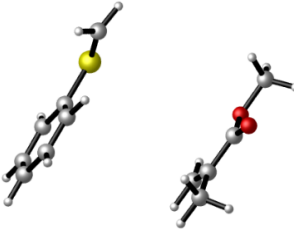
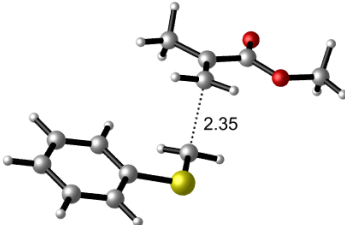
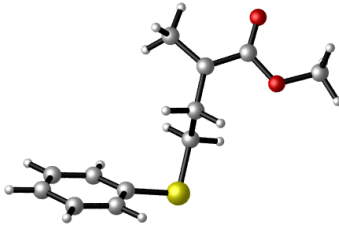
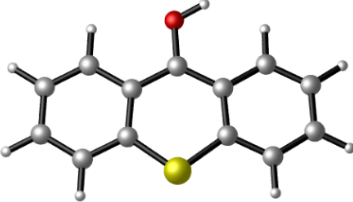
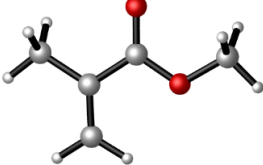
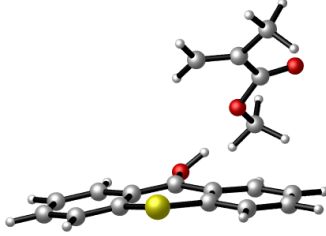
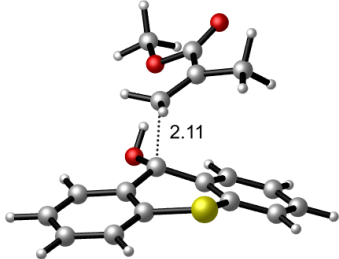
Name	Structure
Reactant 1	
Reactant 2	
Pre-Reactive Complex	
Transition State	
Intermediate	

Table A.12. Optimized ground state geometries of PHS_{exo} radical attack to MMA
(B3LYP/6-31+G(d,p) for S: 6-311++G(3df,3pd) in DMF).

Name	Structure
Reactant 1	
Reactant 2	
Pre-Reactive Complex	
Transition State	
Intermediate	

Endocyclic radical of thioxanthone have possessed similar characteristic with the endocyclic thioxanthone acetic acid derived radicals. A non-planar bended butterfly shape of the non-functional thioxanthone core has been re-observed (Table A.13).

Table A.13. Optimized ground state geometries of TX_{endo} radical attack to MMA (B3LYP/6-31+G(d,p) for S: 6-311++G(3df,3pd) in DMF).

Name	Structure
Reactant 1	
Reactant 2	
Pre-Reactive Complex	
Transition State	
Intermediate	